Sustainable
Energy & Fuels

ROYAL SOCIETY
OF CHEMISTRY

REVIEW

View Article Online
View Journal | View Issue

Check for updates

Cite this: *Sustainable Energy Fuels*, 2025, **9**, 3981

Received 14th April 2025
Accepted 3rd June 2025

DOI: 10.1039/d5se00526d

rsc.li/sustainable-energy

Cerium oxide-based electrolytes for low- and intermediate-temperature solid oxide fuel cells: state of the art, challenges and future prospects

Paramvir Kaur and K. Singh *

Solid oxide fuel cells (SOFCs) are important, efficient, and environmentally friendly energy conversion devices that also serve as solid oxide electrolysers, producing hydrogen and oxygen by reversing chemical reactions. Research and development of electrode and electrolyte materials is still very much needed for their efficient working in low (≤650 °C) and intermediate (650–850 °C) temperature regimes. The present article reviews undoped and doped ceria-based electrolytes in light of processing parameters such as synthesis methods, sintering time, temperature and different doping strategies. The article focuses primarily on the various factors that affect the conductivity of ceria-based electrolytes. Different approaches to enhance the conductivity and improve the cell parameters have also been discussed. Conclusion, challenges and direction for further research are also provided at the end of this article.

1. Introduction

Electricity and water are the basic amenities for the sustainable development of society. However, with the depletion of resources and the increasing population, there is a need to produce clean energy with less carbon and unprocessed waste. The most sought-after way to reduce carbon footprints and meet global energy demands is by using renewable, cleaner, greener energy sources. Hydrogen-based energy sources are an alternative to conventional fuels, such as natural gas, coal, fossil fuels, *etc.* There are many different sources of hydrogen production based on which they are colour-coded, as shown in Fig. 1.[1,2] Green hydrogen is produced from renewable energy sources and produces zero greenhouse gas emissions. Energy conversion devices, *i.e.*, solid oxide fuel cells (SOFCs), utilise green hydrogen as a fuel, and solid oxide electrolysis cells (SOECs) produce green hydrogen.[3,4]

Department of Physics and Material Science, Thapar Institute of Engineering and Technology (Deemed to be University), Patiala 147004, Punjab, India. E-mail: kusingh@thapar.edu

Paramvir Kaur

Dr Paramvir Kaur received an MSc (Honours School) degree in Physics from Panjab University, Chandigarh, in 2014. She was awarded a PhD degree in 2022 by the Department of Physics and Materials Science, Thapar Institute of Engineering and Technology (Deemed to be University), Patiala, Punjab, India. She has worked as a Project Associate on a DST-funded Hydrogen and Fuel Cell-2018 project. Her research focuses on developing perovskite-structured oxides for solid oxide fuel cells. Her work is published in reputed SCI journals such as Ionics and Ceramics International. She has also authored a chapter in a book published by the Academic Press.

K. Singh

Dr Kulvir Singh is a Professor at the Department of Physics and Materials Science, Thapar Institute of Engineering and Technology (Deemed to be University), Patiala, Punjab, India. He received his PhD degree from HPU Shimla in 1995 and later worked as a guest scientist at Forschungszentrum Jülich, Germany. His current research interests are developing ceramic materials for solid oxide fuel cells, batteries, and biomaterials. He also specialises in the development of glasses and glass ceramics. As a reviewer for several high-impact journals, he has authored over 260 research papers, with more than 8790 citations and an h-index of 45.

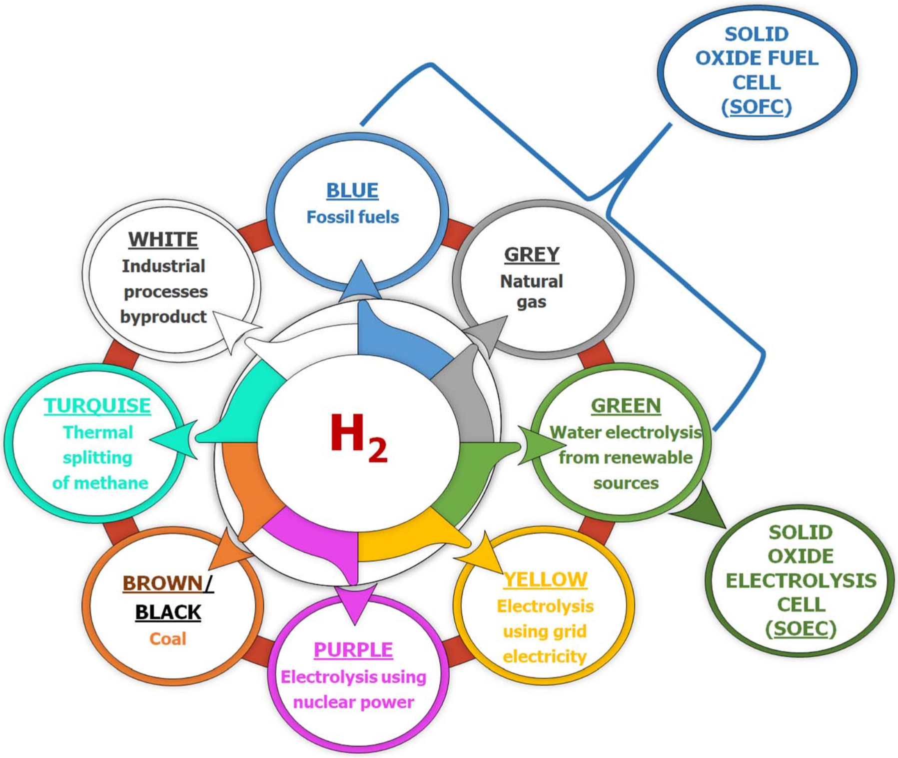

Fig. 1 Sources of hydrogen production and technological applications of green hydrogen.

SOFCs are efficient electrochemical energy conversion devices that produce electricity through a chemical reaction between the fuel (H_2) and air. With fuel flexibility, SOFCs are good candidates for electricity production, having the highest efficiency compared to other fuel cells.[5–8] Additionally, SOFCs are also being used for water production in space missions. Thus, SOFCs could be a future energy source and a strategic source of water production. A single unit of SOFCs consists of two electrodes (anode and cathode) and an electrolyte, having an output of only ~1 volt (V) and power density <2 W cm^{-2}. Therefore, multiple single cells are connected using (metallic or ceramic) interconnects to enhance overall electricity production. The design of SOFCs also incorporates an additional component, such as a glass sealant, in the case of the planar configuration.[9,10]

SOFCs are multipurpose devices that can also be used as electrolysers, *i.e.*, SOECs, to produce hydrogen and oxygen by reversing the reactions to split water into its constituent gases.[11–14] The diagrammatic illustration of SOFCs *versus* SOECs is shown in Fig. 2(a) and (b). In SOFCs, air or oxygen is fed to the cathode and is converted into oxide ions. These oxide ions travel through the electrolyte towards the anode, where they react with the fuel (H_2) to form water (H_2O).[15] The reactions that occur at the electrodes are given as follows:

$$\text{Cathode: } O_2 + 4e^- \rightarrow 2O^{2-} \tag{1}$$

$$\text{Anode: } 2H_2 + 2O^{2-} \rightarrow 2H_2O + 4e^- \tag{2}$$

$$\text{Overall: } 2H_2 + O_2 \rightarrow 2H_2O \tag{3}$$

On the other hand, in the case of SOECs, steam (H_2O) is fed to the cathode and electricity is applied. At the cathode–electrolyte interface, H_2O decomposes into H_2 and O^{2-}. H_2 gas travels through the pores of the cathode to its surface, where it is collected. The O^{2-} ions travel through the electrolyte towards the anode, and at the anode–electrolyte interface, O^{2-} gets oxidized into O_2 gas. The reactions occurring at SOEC electrodes are as follows:[16]

$$\text{Cathode: } H_2O + 2e^- \rightarrow H_2 + O^{2-} \tag{4}$$

$$\text{Anode: } O^{2-} \rightarrow 1/2O_2 + 2e^- \tag{5}$$

$$\text{Overall: } H_2O_{\text{cathode}} \rightarrow H_{2\ \text{cathode}} + 1/2O_{2\ \text{anode}} \tag{6}$$

Therefore, the same device can also produce hydrogen and oxygen. The hydrogen produced from SOECs that use electricity from renewable sources is known as green hydrogen and can be stored in any form: solid, liquid or gas. However, solid-state storage provides many benefits, such as higher volumetric energy density than other storage methods.

In addition to direct biogas and many other fuels, carbon monoxide can also be used in SOFCs. It is converted into less dangerous carbon dioxide during the operation of SOFCs. In fact, oxygen could also be used for many applications, particularly in the medical field, due to its purity, using both these

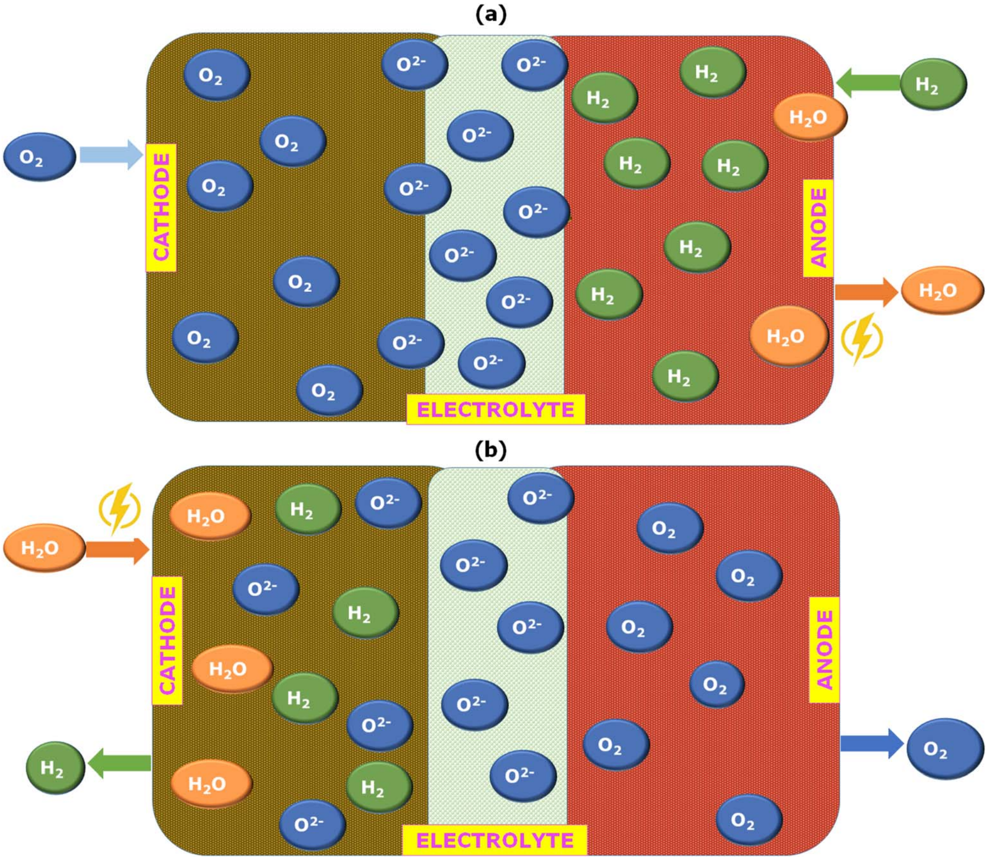

Fig. 2 A schematic illustration of the working of (a) SOFC and (b) SOEC.

operations (SOFCs and SOECs).[17,18] It is a fact that once a technology is developed in one device, others can be modified slightly and used for various purposes. So much research is going on to develop this technology in parallel to other devices, such as batteries, supercapacitors, *etc.*, for use in different applications.[19] Many excellent reviews are available on materials development for various components of SOFC technology.[7,20–25]

The present article focuses mainly on developing electrolyte materials since they are integral to SOFCs and SOECs. An electrolyte is a medium through which ions are conducted from one electrode to another, and the dispersion of anions and cations at an applied potential is responsible for current generation. In fact, the overall device resistance also depends on the ionic flow through the electrolyte. Different fuel cells are also named after the type of electrolyte used (molten carbonate fuel cells, alkaline fuel cells, polymer electrolyte membrane fuel cells, direct methanol fuel cells, phosphoric acid fuel cells, solid oxide fuel cells and reversible fuel cells). Solid electrolytes offer many advantages over aqueous electrolytes and can be used in many applications.[26] Even the temperature categorisation of SOFCs is based on the operating temperature of the electrolyte, *i.e.*, high-temperature (HT-SOFC): 850–1000 °C, intermediate-temperature (IT-SOFC): 650–850 °C and low-temperature (LT-SOFC): <650 °C.

Ceramic materials are predominantly used for SOFCs or SOECs as electrodes and electrolytes. Ceramic materials with high chemical stability, good mechanical strength, and low activation energy (E_a) for ionic conduction are required to qualify as electrolyte materials. Materials with good relative density ($\sim$>95%) preclude open porosity and avoid reactant crossover from the anode to the cathode and *vice versa*. The material requirements for different SOFC components are clearly discussed in the literature.[20,27–36] As mentioned earlier, the conducting properties of electrolyte materials are of utmost importance. Therefore, in the present article, the primary focus is to analyse the conductivity of electrolyte materials and correlate other properties with conductivity.

2. Electrolyte materials for SOFCs

Since the inception of SOFCs, many materials such as fluorite-structured ZrO_2, CeO_2, Bi_2O_3-based oxides, perovskite-structured $LaGaO_3$, $SrTiO_3$, $Bi_4V_2O_{11}$, $La_2Mo_2O_9$, $Ba_2In_2O_5$ oxides, brownmillerite and pyrochlore-structured materials have been investigated and developed for use as electrolytes for SOFCs.[20,37–45] SOFC electrolytes could be oxygen, proton or dual (oxygen and proton) conducting.

Eight mol% yttria stabilised zirconia (8-YSZ) is a widely used oxide ion electrolyte material in HT-SOFCs since it is reported to have an ionic conductivity of 0.1 S cm^{-1} at 1000 °C. It also exhibits good mechanical properties without compromising the stability of the cell and the durability of its performance.[30,46]

However, in IT- and LT-SOFCs, the ionic conductivity of 8-YSZ decreases drastically to ~7.2×10^{-4} S cm^{-1} at 500 °C.[47] This issue of poor ionic conduction can be resolved by reducing the thickness of the electrolyte or by finding a substitute for YSZ.[48–50] Other than YSZ, scandia stabilised zirconia (ScSZ) is also known to exhibit high ionic conductivity. The close ionic radii of Zr^{4+} and Sc^{3+} decrease the association enthalpy of the defects, resulting in higher conductivity for ScSZ, *i.e.*, 3×10^{-1} S cm^{-1} at 1000 °C, than that of YSZ. However, the high cost and rarity of scandia limit the use of ScSZ, and the reaction of zirconia with strontium or lanthanum present in the cathode limits their use as electrolytes.[51,52]

Compared to YSZ and ScSZ, bismuth-based fluorite-structured materials (δ-Bi_2O_3) exhibit the highest oxygen ionic conductivity. This is due to a high concentration of oxygen vacancies and easy anion mobility in these electrolytes. However, the ionic conduction decreases significantly in these oxides when the operating temperature is lowered. A large dopant concentration is used to stabilise these oxides. Gd, La, Cu, Ti, Al, Ga, *etc.*, are commonly used dopants.[43,44,53–55] The dopant ionic radius and polarizability affect the conductivity and stability of these bismuth oxide-based electrolytes. γ-$Bi_4V_2O_{11}$ doped with transition metals, *i.e.*, BIMEVOX, demonstrates high ionic conductivity and higher stability at 600 °C. It exhibits three polymorphs (α, β, and γ) with respect to temperature, and the higher temperature γ-phase has a higher oxygen vacancy disorder in the O–V polyhedra. The major drawback of $Bi_4V_2O_{11}$ is the slow phase transformation (δ → α) occurring between 500 and 600 °C, which decreases its conductivity and limits its usage in LT- and IT-SOFCs. Additionally, Bi_2O_3 decomposes into metallic Bi in reducing environments, has poor mechanical strength and a high coefficient of thermal expansion (CTE) and is chemically reactive with other SOFC components, thus limiting its usage as electrolyte.[52,56–60]

Perovskite-based oxides are another popular electrolyte material choice with high SOFC performance. At 500 °C, the oxide ion conductivity of $Sr_{0.55}Na_{0.45}SiO_{2.755}$ is > 10^{-2} S cm^{-1}, having an activation energy of 0.3 eV. A SOFC with $Sr_{0.55}Na_{0.45}SiO_{2.755}$ electrolyte has high power densities of 431 and 213 mW cm^{-2} at 600 and 500 °C, respectively. It is a promising SOFC electrolyte candidate with activation energy that is much lower than that of other commonly used oxygen ion conductors and high power density.[61] Mo-substituted $SrFeO_3$ achieved power densities between 0.24 and 1.12 W cm^{-2} across 600–800 °C. A SOFC single cell employing a $SrFe_{0.93}Mo_{0.07}O_{3-\delta}$ cathode exhibited excellent operational stability over 270 h at 700 °C.[62] Lanthanum-based oxides such as $LaAlO_3$, $LaSrO_3$, $LaInO_3$, $LaScO_3$, $LaYO_3$, *etc.*, exhibit minimum electronic conduction and high stability at lower operating temperatures. Adding Co, Ni, or Bi in small quantities at the gallium site and co-doping at the La and Ga sites enhances ionic conductivity.[63–67] However, phase instability, gallium volatilisation at high temperatures, and chemical incompatibility with nickel limit the use of these materials.[20,68]

Fluorite-structured electrolytes offer many advantages over traditionally used materials; therefore, they are widely used as SOFC electrolyte materials. The following sub-section discusses ceria-based electrolytes in detail.

2.1. Ceria-based electrolytes

Cerium dioxide (CeO_2) with different dopants is used in many applications.[69–73] As mentioned in the introduction section, the primary focus of the present review is on the various parameters affecting the conductivity of CeO_2 and discussing its applicability as an electrolyte for SOFCs. CeO_2, commonly known as ceria, has a fluorite structure (AX_2) with A as the cation and X as the anion. Structurally, each Ce^{4+} cation is coordinated to eight O^{2-} anions. Each O^{2-} anion is located at the tetrahedral interstices of four Ce^{2+} cations.[74] The electronic configuration of cerium is [Xe] $4f^26s^2$ with two common valence states, cerium(III) and cerium(IV). A detailed overview of the structure of CeO_2 is given by Sun *et al.* and shown in Fig. 3.[69] The fluorite structure with the space group *Fm3m* is stable over a wide temperature range (room temperature-2400 °C). Unlike ZrO_2, Bi_2O_3, *etc.*, electrolytes, the phase transition does not occur up to their melting point. In some electrolytes, it can be stabilised using different dopants and their concentration. The task is stabilising the high conducting phase, such as γ-phase in $Bi_4V_2O_{11}$ and the cubic phase of ZrO_2, to use as electrolytes in SOFC technology. In the case of CeO_2, the cubic phase already exists with unoccupied octahedral sites necessary for oxide ion diffusion. The cationic or anionic vacancies can be further increased by introducing appropriate dopants and their concentrations. These vacancies are required since ionic conduction occurs *via* the vacancy diffusion mechanism.

Pure CeO_2 ceramic is a poor oxide ion conductor (~0.24×10^{-3} S cm^{-1} at 700 °C) since it lacks sufficient vacant sites for oxide ion transport, as shown in Fig. 3(a).[75–77] At lower temperatures, the reduction of Ce^{4+} to Ce^{3+} leads to the generation of more oxygen vacancies and electrons. These electrons act as polarons as they are localised to Ce^{3+}; therefore, electron hopping between Ce^{3+} and Ce^{4+} leads to n-type conductivity, which reduces the open circuit voltage (OCV) to a large extent. This causes the electrolyte to be a mixed ionic-electronic conductor rather than a pure ionic conductor. Also, the larger ionic radius of Ce^{3+} ($r_{\text{ionic}} = 1.01$ Å) than Ce^{4+} ($r_{\text{ionic}} = 0.87$ Å) obstructs the migration of O^{2-} ions, thereby reducing the ionic conductivity in this temperature range.[78,79] Additionally, the electrolyte should be a purely ionic conductor; therefore, the presence of electrons in the electrolyte hinders its performance and poses a risk of short-circuiting. Unwanted reactions at the electrode–electrolyte interface lead to the degradation of the electrolyte, reducing the device's efficiency.[80]

The ionic radii of the dopant cation significantly affect the ionic conductivity of the electrolyte. Doping with larger cation sizes can block the migration of vacancies, leading to higher E_a of ionic conduction. Thus, a better strategy is to have the dopant and host cation size comparable for better ionic conductivity. Additionally, to sufficiently increase the ionic conductivity of CeO_2, doping of lower valence cations is done to increase the oxygen vacancy concentration.[81] When a lower valence cation (aliovalent) replaces a higher valence cation, oxide ion vacancies

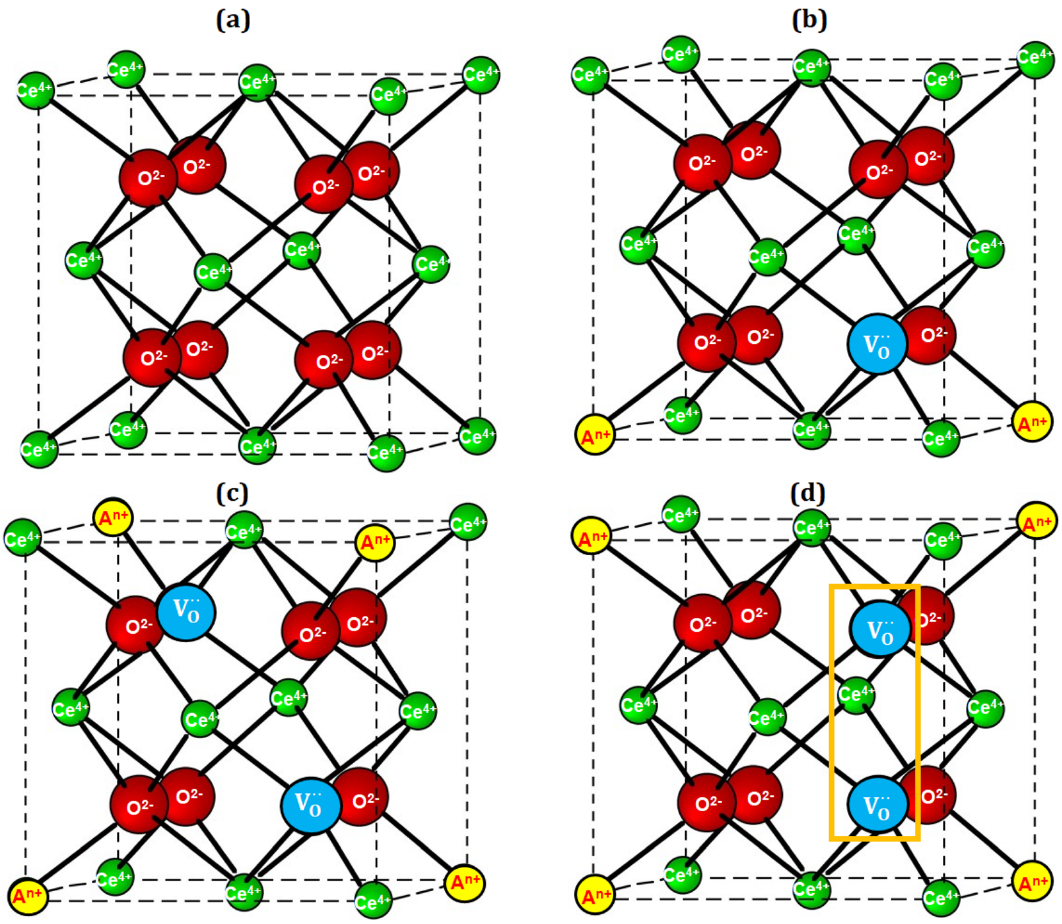

Fig. 3 Schematic representation of the effect of doping on the crystal structure of CeO_2. (a) The undoped CeO_2 structure. (b) and (c) Ce^{4+} replacement by lower valence cations (A^{n+}: $n = 3, 2, 1$) leads to the formation of disordered oxide ion vacancies ($V_O^{\cdot\cdot}$), and (d) vacancy clustering. The higher number of vacancy clusters lowers the ionic mobility, which decreases the ionic conductivity.

are introduced to maintain overall charge neutrality. This is when the fluorite structure of Ce^{4+} becomes distorted. It allows transportation of the oxide ions on thermal activation through the lattice by hopping from one crystal lattice site to its neighbouring vacant site, as shown in Fig. 3(b) and (c). Therefore, aliovalent doping is better than isovalent doping for enhancing oxide ion conductivity in CeO_2 due to defect engineering. Replacement by a dopant of different ionic radii (aliovalent) creates point defects (vacancies) in the system. These vacancies expedite the ionic conduction in CeO_2. Dopants cause unit cell expansion and contraction *via* altering the average size of cations and the lengthening or contracting of the cation–oxygen bond length, which are determined by the host's and dopant's oxidation states and their ionic radius. The unit cell expands or contracts due to both factors working together.[22] A smaller ionic radius causes a compressive strain responsible for charge neutrality. Therefore, aliovalent doping in CeO_2 causes a local lattice strain, which facilitates the formation and migration of oxygen vacancies.

Aliovalent-doped ceria has received significant attention due to its superior ionic conductivity between 500 and 800 °C in air.[82,83] Sr^{2+} and Ca^{2+} doping improve the oxide ion conductivity of ceria-based electrolytes significantly. Sr^{2+} doped CeO_2, $Ce_{0.925}Sr_{0.075}O_{2-\delta}$ has a relative density, conductivity and power density of 97%, 6.46×10^{-3} S cm^{-1} and 89 mW cm^{-2}, respectively, at 600 °C. Here, Sr^{2+} doping serves a dual purpose. It creates oxygen vacancies in CeO_2 and acts as a sintering aid.[84] Doping of $Ce_{0.8}Sm_{0.2}O_{2-\delta}$ with Bi^{3+}, Mg^{2+} and Li^{+} results in a higher conductivity of 0.089×10^{-3}, 0.39×10^{-3}, and 0.13×10^{-3} S cm^{-1} and power density of 716, 929 and 1097 mW cm^{-2} in comparison to undoped $Ce_{0.8}Sm_{0.2}O_{2-\delta}$, having a conductivity and power density of 0.11×10^{-3} S cm^{-1} and 281.5 mW cm^{-2}, respectively. The higher conductivity and power density in the doped samples were attributed to the small amount of impurities in the ceria lattice.[85] Generally, alkaline earth dopants are cost-effective, readily available and eco-friendly. The small amount of these oxides works as sintering aids when used as dopants in CeO_2 electrolytes. However, their solid solubility is limited compared to rare earth dopants, leading to secondary phase formations. Additionally, larger ionic radii of some of the alkaline earth dopants cause the lattice to expand and decrease the ionic mobility.[86]

Apart from alkaline earth dopants, there is extensive literature on doping ceria with rare-earth elements such as La^{3+},

Nd^{3+}, Gd^{3+}, Y^{3+}, Sm^{3+}, Eu^{3+}, *etc.*, since they exhibit higher bulk ionic conductivities than other elements.[27,87–90] Gd-doped ceria (GDC) has been a popular electrolyte material since it has higher conductivity (10^{-2} S cm^{-1}) than YSZ (10^{-3} S cm^{-1}) at 500 °C. This is because it reduces the reduction of Ce, which restricts electronic conduction. Also, the ionic radius of Ce^{4+} ($r_{\text{ionic}} = 0.87$ Å) is greater than that of Zr^{4+} ($r_{\text{ionic}} = 0.72$ Å); therefore, CeO_2 has a more open fluorite structure than YSZ. It leads to an increase in the Ce–O bond lengths and a decrease in the E_a, which is responsible for the increase in the ionic conductivity of CeO_2.[20,91–93] Similarly, the ionic radii of Gd^{3+} ($r_{\text{ionic}} = 0.938$ Å) and Sm^{3+} ($r_{\text{ionic}} = 0.958$ Å) are closer to that of Ce^{4+} ($r_{\text{ionic}} = 0.87$ Å); therefore, these dopants show maximum ionic conductivity with minimum lattice distortion due to size difference. The differences in ionic sizes of the dopants influence the localisation of oxygen vacancies by defect association, formation of secondary phases, *etc.*, all of which modify grain and grain-boundary conductivity. The conductivity of divalent ions is less than that of trivalent ions because of the larger ionic radius mismatch between divalent ions and cerium ions (Ce^{4+}).[20,94,95]

Doping can be done only up to a specific concentration of the dopant. It happens for several reasons, such as vacancy clustering, vacancy repulsion and a rampant increase in the solid solubility limit. As reported in the literature, the ionic conductivity of doped ceria can reach a maximum only up to a certain extent of dopant concentration. After this limit, there is an increase in the defect interactions that gives rise to the clustering of vacancies, after which the mobile ions reduce, as shown in Fig. 3(d). Larger clusters require more atoms that need to be displaced for ionic motion. This requires larger E_a, and there is a decrease in the ionic conductivity.[96,97] The solid solubility limits of some commonly used dopants are given in Fig. 4. The maximum solubility limit is observed where the ionic radii of dopants are close to that of Ce^{4+}, after which there is formation of secondary phases which are usually segregated along the grain boundaries, hindering the movement of mobile ions.[98–100]

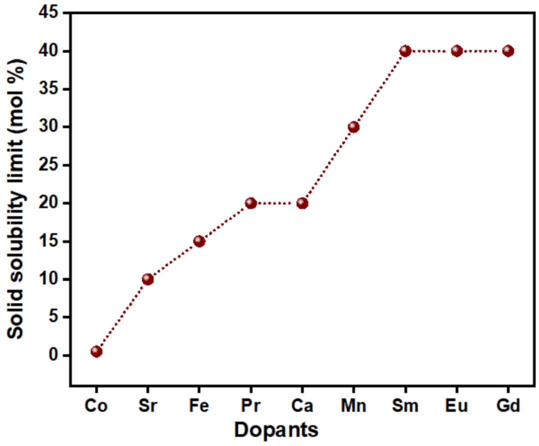

Fig. 4 Solid solubility limits of common dopants used in CeO_2 synthesised using the solid-state reaction and wet-chemical routes.[98–100]

The following thermodynamic relations are responsible for governing the solubility limit of the dopants at equilibrium:

$$\Delta G = \Delta H - T\Delta S \tag{7}$$

$$\Delta G = \frac{1}{2} RT \ln pO_2 \tag{8}$$

$$\frac{1}{2}\ln pO_2 = \frac{\Delta H}{RT} - \frac{\Delta S}{R}\bigg|\delta = \text{constant} \tag{9}$$

where G, H, T, S, R, and pO_2 refer to Gibbs free energy, enthalpy, temperature and entropy, gas constant and oxygen partial pressure, respectively. Δ refers to the changes in the thermodynamic quantities, and δ represents the oxygen non-stoichiometry. The slope and intercept of $\ln pO_2$ *versus* $1/T$ for a constant δ give ΔH and ΔS as a function of δ. The Gibbs free energy must be negative for a dopant to be completely soluble. This is because entropy always increases with temperature. Increased atomic mobility at elevated temperatures facilitates dopant diffusion and incorporation into thermodynamically favourable lattice sites, promoting equilibrium solubility. In contrast, low temperatures suppress diffusion kinetics, limiting dopant activation and incorporation into the crystal structure.[101–103]

On the whole, the dopant type and concentration affect the electrolyte performance. Higher and lower ionic radius dopants introduce cationic and oxide ion vacancies, respectively. Dopants only up to a certain limit can be introduced in the system since higher concentrations lead to the formation of secondary phases that disrupt the conductivity of the electrolyte. Several factors affect the ionic conductivity of the electrolytes, many of which are discussed in the following sections.

3. Role of processing parameters in conductivity and other properties

The selection of starting materials is essential for better homogeneity of a mixture. It is imperative to understand the starting chemicals used for different synthesis methods. Generally, oxides and carbides are used as starting materials for the solid-state reaction and nitrates are used for the sol–gel (chemical wet) method. Chemicals used for synthesis can vary in purity depending on the studied property. For example, point defects (oxide vacancies) are introduced into the system for better ionic conduction. Raw materials with lower purity can provide the necessary defects in this case. Apart from the selection of raw materials, microstructural uniformity, particle size, grain growth, grain size and shape, density, sintering time, and temperature are also important for different synthesis methods.[104]

For a homogeneous mixture, it is necessary to consider the grain size of the composition, which varies from one synthesis method to another. In powder methods, the mixing/ball milling of powders is done before sintering. The difference in grain size may be attributed to the particles' composition, which introduces defects and internal stress to their structure.[105] The effect of calcining composition, $Li_{6.4}Fe_{0.2}La_3Zr_2O_{12}$, using the solid-state and sol–gel methods was studied by Paulus *et al.*[106] A mixture of the cubic and tetragonal structures was observed in the solid-state reaction method due to the inhomogeneous distribution of iron in the sample. However, samples calcined using the sol–gel method yielded homogeneous, single-phase cubic structures. Calcination by sol–gel also decreased the sintering time by 2 hours. The sample exhibited a total ionic conductivity of 1.82×10^{-3} S cm^{-1} at 25 °C, the highest for garnet-related materials. Therefore, the exact composition synthesised using different techniques yields different results.

Control over the grain size is essential for the dielectric response of CeO_2. There are several ways to control the grain size: ball-milling, varying sintering temperature and doping.[107] Smaller grains have a more intense dielectric response. Due to the greater concentration of grain boundaries in smaller grains, the effect of grain size is primarily caused by increased surface stress.[108,109] Cationic diffusion governs the grain boundary mobility through an interstitial mechanism that is influenced by oxygen vacancies.[110] Densification occurs by grain boundary diffusion rather than lattice diffusion. Sintering is dependent on the reduction of the excess surface energy, in which the following equation gives the flux of atoms (J) along a grain boundary:

$$J = MC\nabla\mu \tag{10}$$

where M is the mobility of the atoms along the grain boundary, C is the vacancy concentration, and $\nabla\mu$ is the gradient in the chemical potential between the atoms in the materials and the neck of adjacent particles.[111,112] Dopants that increase any of these parameters lead to lower sintering temperatures.

Processing parameters play an important role in modifying various properties of ceramic materials.[113] The dopant composition, the thickness of the electrolyte, the microstructure, the sintering temperature, *etc.*, affect the cell's overall performance as illustrated in Fig. 5. The shape and size of grains potentially affect the interaction of dopant-oxygen vacancies, affecting ion migration and ionic conductivity. The microstructure can have regularly or irregularly arranged grains of different shapes, such as hexagonal, polygonal, globular, *etc.* Finer grain sizes lead to more grain boundaries necessary for ionic conduction. As reported in the literature, CeO_2 generally deviates from the stoichiometric composition by releasing gaseous oxygen; this process could also be monitored from the morphology of the samples (bubbles on the surface).[114,115] Surface modifications (synthesis techniques and sintering temperature) can significantly enhance the ionic conductivity of CeO_2 without using dopants. Hydrogen treatment leads to the formation of chemical defects in CeO_2, facilitating the reduction of Ce^{4+} to Ce^{3+}. Surface-modified $CeO_{2-\delta}$ shows a conductivity and power density of 0.1 S cm^{-1} and 660 mW cm^{-2} at 550 °C.[116]

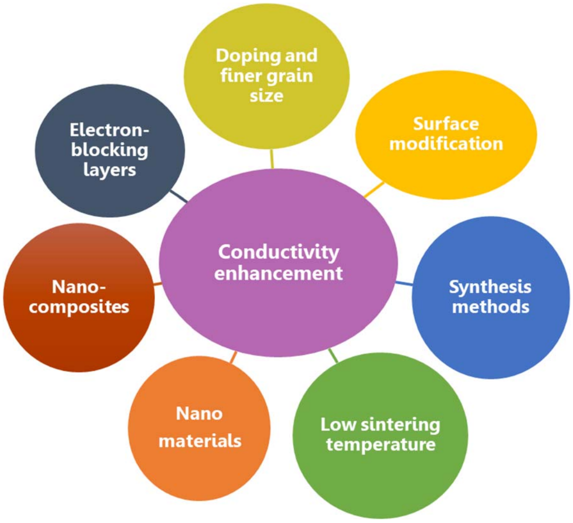

Fig. 5 Factors that increase the ionic conductivity of CeO_2-based electrolytes.

Synthesis methods play an essential role in the densification of the microstructure, affecting the conducting properties of SOFCs.[117] Different methods have been used to synthesise doped CeO_2, such as co-precipitation, hydrothermal, sol–gel and solution combustion.[117–123] A comparative diagrammatic representation of the high- and low-temperature synthesis methods is given in Fig. 6. Synthesis of calcium-doped ceria electrolyte using two different synthesis methods, the solid-state reaction and sol–gel, resulted in varying microstructures. The sol–gel method resulted in well-defined homogeneous grains compared with the solid-state reaction method. Furthermore, the samples synthesised using sol–gel exhibited better conductivity than those synthesised by the solid-state reaction method. Therefore, the low-temperature synthesis method yielded better results.[124]

Sol–gel, co-precipitation, hydrothermal, *etc.*, are some low-temperature synthesis methods. Sol–gel is based on the polymerisation of molecular precursors. It involves the preparation of inorganic polymers or ceramics from a solution through a transformation from liquid precursors into a sol and then into a network structure called a gel. This high-purity process leads to a homogenised composition.[125,126] Smaller crystallite size, the low energy band gap value, and the homogeneous distribution of Sm^{3+} in the ceria lattice, with its high ionic mobility, accounted for the high conductivity of $(CeO_2)_{0.96}Sm_{0.04}$ solid electrolyte synthesised by the sol–gel process.[127]

CeO_2-based electrolytes exhibit rapid grain growth when sintered at high temperatures. This leads to poor mechanical stability, partial reduction of Ce^{4+} to Ce^{3+}, undesirable chemical expansion, high energy cost, phase diffusion and chemical interaction between the components, thus affecting the electrochemical performance of the cell.[49,128] Therefore, there has been a shift in the synthesis of CeO_2 towards lower-temperature methods. The literature reports far more publications on the low-temperature synthesis of CeO_2 electrolytes than the high-temperature methods. Low-temperature methods are generally wet chemical methods. They differ from powder methods in that the starting materials, in this case, are synthetically derived. This reduces the additional step of removing the impurities. Synthetically derived materials have uniform grain sizes and high purity without any agglomerates.

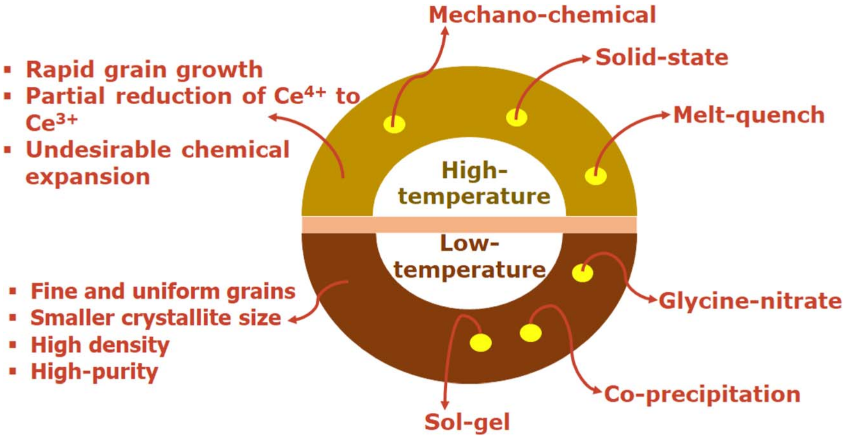

Fig. 6 Comparative representation of the high- and low-temperature synthesis methods.

Accardo *et al.* reported that the conductivity of 20 mol% of GDC is 1.9×10^{-2} to 5.5×10^{-2} S cm^{-1} at 600 °C and 800 °C, respectively. However, doping of Bi^{3+} increased the conductivity of GDC to 3.1×10^{-2}-1.7×10^{-1} S cm^{-1} between 600 and 800 °C. The dense microstructure of the GDC pellets is composed of highly packed spherical grains due to the decrease in particle size (~30 and 28 nm).[117,129] In another case, GDC powders were prepared using three complexing agents/fuels (ethylene glycol, glycerol, and tartaric acid) with sinterability strongly dependent on the microstructure, which in turn depended on the processing route.[130] Low-temperature methods usually result in crystallite and grain sizes in the nanometer and micrometre range, respectively. Smaller crystallite sizes favour better crystallinity with densities >90%. Single-phase $Ce_{0.8}Sm_{0.2}O_{1.9}$ synthesised by sol–gel with gelatin as a polymerising agent exhibited a dense, regular polygonal microstructure with a density, crystallite and particle size of > 97%, 12 nm and 15 µm, respectively. The conductivity of the samples was in the order of 10^{-3} S cm^{-1}, and the E_a was ~0.94 eV at 600 °C.[131]

In the case of doped ceria electrolytes, high ionic conductivity is essentially due to low E_a, which, in turn, is related to an optimal balance between elastic and electronic coulombic defect interactions. The Arrhenius curve is instrumental in identifying the E_a based on the temperature range. As shown in Fig. 7, the Arrhenius curve is fitted separately with two lines, one for the high-temperature range and the other for the low-temperature range. The low-temperature line is slightly curved since the vacancies are temperature-dependent. In the low-temperature range, the E_a is the sum of enthalpies, association (ΔH_a) and migration (ΔH_m) for conduction, while for the high-temperature range, it is equal to only the ΔH_m. This is because most oxygen vacancies are free to migrate in the high-temperature region. It is worth noting that for electrolytes to work in the low-temperature region, ΔH_a should be a minimum.[132–135]

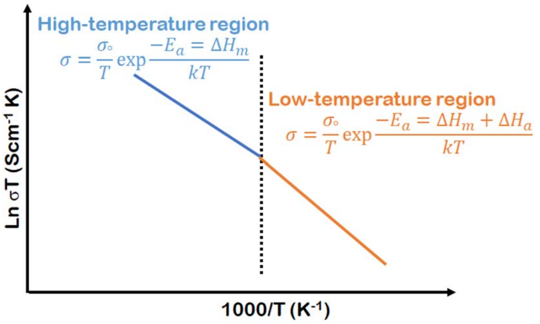

Fig. 7 Representative Arrhenius curve. The dotted line represents the change in the type of conduction.

Other processes, such as microwave sintering, can further enhance densification. In a particular case, GDC nanoparticles with lithium as an additional dopant were used as a liquid-phase sintering aid during synthesis by the co-precipitation method. Furthermore, microwave sintering resulted in a decrease in the sintering temperature to 600 °C. The grain sizes of the Li-doped samples exhibited a grain size of 150 nm compared to pristine GDC (30 nm). At 600 °C, Li-doped samples showed an ionic conductivity of 1×10^{-2} S cm^{-1} in air with an E_a of 0.53 eV.[136] As discussed before, the partial electronic conductivity at high temperatures is related to the reduction of Ce^{4+} to Ce^{3+}. The electrons thus created participate in the conduction process through the small polaron hopping mechanism. The decrease in the OCV due to this partial electronic conductivity also lowers the cell's overall efficiency and might lead to an electrical short-circuit. This is a paramount concern when synthesising doped ceria electrolytes at high temperatures. Therefore, many researchers are synthesising doped ceria electrolytes at low temperatures. Out of the various synthesis methods listed in Table 1, sol–gel and auto-combustion methods result in highly dense (≥95%) electrolytes with good conductivity values (~10^{-1} S cm^{-1}).

Sometimes, liquid phase formation occurs at high temperatures, where a liquid phase is formed during the sintering process that coexists with the solid particles. The liquid during the liquid-phase sintering eliminates the solid–vapour interface. With further sintering, the driving force for the densification results from the decreasing liquid–vapour pore surface

Table 1 Comparative analysis of different ceria-based electrolytes

Composition	Synthesis method	ρ_{rel} (%)	σ (S cm^{-1})	E_a (eV)	References
$Ce_{0.8}Gd_{0.2}O_{1.95}$	Combustion	—	3.34×10^{-3} (680 °C)	—	105
$Ce_{0.9}Gd_{0.1}O_{1.95}$	Sol–gel combustion	95	1.67×10^{-2} (600 °C)	0.81	92
$Ce_{0.8}Ca_{0.2}O_{1.95}$	Combustion	—	6.90×10^{-4} (680 °C)	—	105
$Ce_{0.9}Dy_{0.1}O_{2-\delta}$	Solid state reaction	—	$1 \times 10^{-1.91}$ (650 °C)	0.71	115
$Ce_{0.8}Nd_{0.2}O_{1.9}$	Molten salt	92	0.15×10^{-2} (600 °C)	0.87	142
$Ce_{0.83}Er_{0.17}O_2$	Sol–gel	—	1.57×10^{-3} (700 °C)	—	143
$Ce_{0.8}Yb_{0.2}O_{1.9}$	Solid state reaction	94	1.30×10^{-2} (800 °C)	1.07	144
$Ce_{0.9}Pr_{0.1}O_2$	EDTA citrate	—	1.21×10^{-2} (700 °C)	1.28	109
$Ce_{0.9}La_{0.1}O_{2-\delta}$	Auto-combustion	—	1.01×10^{-2} (750 °C)	0.70	145
$Ce_{0.8}La_{0.2}O_{2-\delta}$	Co-precipitation	—	0.81×10^{-2} (650 °C)	0.86	165
$Ce_{0.8}Zr_{0.2}O_{2-\delta}$	Co-precipitation	—	0.15×10^{-2} (650 °C)	0.88	158
$Ce_{0.7}Sm_{0.3}O_{1.85}$	Solid state reaction	97	1.6×10^{-3} (500 °C)	0.92	146
$Ce_{0.8}Sm_{0.2}O_{1.95}$	Combustion	—	8.32×10^{-3} (680 °C)	—	105
$Ce_{0.8}Sm_{0.2}O_{2-\delta}$	Sucrose-pectin modified sol–gel	95	1.0×10^{-2} (600 °C)	0.89	134
$Ce_{0.8}Sm_{0.2}O_{1.9}$	Solid state reaction	97	5×10^{-2} (800 °C)	1.03	147
$Ce_{0.95}Sm_{0.05}O_{1.95}$	Auto-combustion	93	3.26×10^{-3} (500 °C)	0.87	148
$Ce_{0.96}Sm_{0.04}O_{1.92}$	Sol–gel	—	0.17×10^{-2} (500 °C)	—	127
$Ce_{0.8}Gd_{0.10}Pr_{0.10}O_{1.90}$	Citric acid nitrate combustion	94	5.1×10^{-2} (750 °C)	0.58	135
$Ce_{0.8}Y_{0.18}La_{0.02}O_{2-\delta}$	Sol–gel	97	5.7×10^{-2} (800 °C)	0.87	150
$Ce_{0.6}Zr_{0.2}La_{0.2}O_{2-\delta}$	Co-precipitation	—	0.32×10^{-2} (650 °C)	0.87	165
$Ce_{0.8}Nd_{0.10}Mg_{0.10}O_{2-\delta}$	Sol–gel	98	26.81×10^{-2} (450 °C)	0.74	152
$Ce_{0.8}Sm_{0.05}Mg_{0.15}O_{2-\delta}$	Solid state reaction	96	1.18×10^{-2} (600 °C)	0.60	153
$Ce_{0.8}Er_{0.1}Gd_{0.1}O_2$	Sol–gel	—	2×10^{-3} (700 °C)	—	165
$Ce_{0.875}Gd_{0.1}Sr_{0.025}O_{1.925}$	Sol–gel combustion	96	1.20×10^{-2} (600 °C)	0.96	154
$Ce_{0.65}Sm_{0.2}Bi_{0.15}O_{1.825}$	Co-precipitation	94	5.6×10^{-2} (800 °C)	0.83	155
$Ce_{0.80}Ba_{0.10}Ga_{0.10}O_{3-\delta}$	Co-precipitation	—	7.1×10^{-2} (650 °C)	0.46	156
$Ce_{0.76}La_{0.08}Pr_{0.08}Sm_{0.08}O_{2-\delta}$	Sol–gel auto combustion	98	1.4×10^{-2} (500 °C)	0.76	151
$Ce_{0.80}Sm_{0.10}Er_{0.05}Ba_{0.05}O_{2-\delta}$	Solid state reaction	89	1.86×10^{-2} (800 °C)	—	157
$Ce_{0.76}Pr_{0.08}Sm_{0.08}Gd_{0.08}O_{2-\delta}$	Sol–gel auto combustion	95	1.86×10^{-2} (600 °C)	0.56	158
$Ce_{0.76}Pr_{0.08}Sm_{0.08}Gd_{0.08}O_{2-\delta}$	Microwave-assisted sol–gel auto-combustion route	98	3.47×10^{-2} (600 °C)	0.69	159
$Ce_{0.82}La_{0.06}Sm_{0.06}Gd_{0.06}O_{2-\delta}$	Sol–gel	91	3.8×10^{-2} (600 °C)	0.59	160
$Ce_{0.8}Sm_{0.2}O_{1.9}\cdot(CuO)_{1.0}$	Combustion	96	1.46×10^{-2} (600 °C)	0.59	149
$[Ce_{0.82}La_{0.06}Sm_{0.06}Gd_{0.06}O_{2-\delta}$-(Li– Na)$_2CO_3]$	Sol–gel	86	4.2×10^{-1} (600 °C)	1.51	161
$[Ce_{0.76}La_{0.08}Pr_{0.08}Sm_{0.08}O_{2-\delta}$-(Li–Na)$_2CO_3]$	Solid state reaction	87	4.6×10^{-1} (600 °C)	1.03	169

area.[137] Sintering aids such as transition metals (cobalt, copper, lithium and iron) are used to increase the mobility of the atoms along the grain boundaries, promoting liquid phase sintering.[111,138,139] A comparison of the sintering aids (Li, Co, Cu, and Fe) used in samarium-doped CeO_2 (SDC) concluded that CuO was the best, as it lowered the sintering temperature between 750 and 1100 °C. CuO also has better relative density and maximum shrinkage rate than other electrolytes. Cobalt-sintered SDC had a more prominent grain size, while FeO had better conductivity than the others.[140] The impact of different dopants (Li, Co, Fe and Mg) on the sintering temperature of $Ce_{0.9}Pr_{0.1}O_2$ showed that the dopants had a different impact on the sintering temperature. Li and Co reduced the sintering temperature, Fe increased it, and Mg had little effect on the sintering temperature. The reduction in the sintering temperature resulted in rapid densification due to the formation of a liquid phase in the grain boundaries of the sample. This is attributed to the diffusion of the liquid phase under capillary action and the rearrangement of grains during the sintering process.[49] Ca doping also acts as a suitable sintering aid, and doping with an appropriate ratio of Gd/Ca also enhances conductivity. $Ce_{0.8}Gd_{0.12}Ca_{0.06}O_{1.87}$ exhibits a relative density of >95% when sintered at 1400 °C, denser than the ceria sintered at 1600 °C. This lowering of sintering temperature is due to grain refining, the modified gel-casting synthesis route, and Ca as a sintering aid. The samples had a conductivity and an E_a of 0.082 S cm^{-1} and 0.786 eV, respectively, at 800 °C. The conductivity increases with increasing Ca content due to the majority of oxygen vacancies being fluid.[141]

Each cell component must be chemically and thermally stable. All the SOFC components must have good chemical compatibility; there should be no or negligible mismatch. If this mismatch persists, it will lead to cell degradation. Also, the components must be stable in both oxidising and reducing oxygen partial pressure atmospheres. During SOFC fabrication, the long duration of operation often leads to mechanical and thermal stress. However, the addition of dopants improves the mechanical strength and leads to an increase in CTE. Therefore, research is needed to balance these properties to avoid any mismatch during operation. The mismatch in CTE among various SOFC components leads to interface delamination; in fact, multiple SOFC components form different interfaces, as shown in our recent review article.[10] Also, the increase in the oxygen vacancies contributes to weakening the binding energy, which increases CTE. In the planar design of SOFCs, electrolytes form interfaces with the cathode, anode and sealants. If the CTE largely differs in every component, a SOFC device will not form. However, with the proper selection of dopants, CTE can be tailored accordingly. In the case of anode-supported SOFCs, the CTE difference between electrolyte and the anode substrate leads to a significant thermoelastic bending of the cells that causes cell fracture in stack assembling.[161–163] La-doped CeO_2 exhibited a CTE of 13.4×10^{-6} per °C without compromising the conductivity (0.81×10^{-2} S cm^{-1} at 650 °C).[164] However, tri-doped ceria, $Ce_{0.76}Pr_{0.08}Sm_{0.08}Gd_{0.08}O_{2-\delta}$, exhibits comparable CTE (13.25×10^{-6} per °C) between 30 and 800 °C.[158]

Mechanical properties must be checked and verified thoroughly for any fuel cell design under all conditions, *i.e.*, operation, start-up, and shutdown. Wettability, joint strength, fracture toughness, elastic modulus, and hardness are some pointers to be checked for SOFC materials. The change in the crystal structure affects the elastic modulus and stiffness of SOFC materials.[165–168] The correlation between electrical and mechanical properties of the $La_{0.90}Sr_{0.10}Ga_{0.8}Mg_{0.2}O_{3-\delta}$ and $La_{0.85}Sr_{0.15}Ga_{0.8}Mg_{0.2}O_{3-\delta}$ ceramics showed that significant segregation of secondary phases occurs at the grain boundaries. This led to a substantial drop in the hardness and grain boundary conductivity, which decreased the total ionic conductivity.[170] An increase in sintering temperature facilitates enhanced grain growth, reducing the grain boundary area per unit volume. Consequently, these grains are less resistant to localised plastic deformation and exhibit poorer hardness.[171]

Enhancement of strength over that of zirconia would lower the likelihood of fracture and enhance ionic conductivity at the same thickness, which would lower ohmic loss. Materials such as ceria would enable highly dependable and energy-efficient SOFCs.[172] It has been observed that ceria-based materials exhibit slightly lower hardness and toughness values compared with commonly used electrolyte materials such as 8-YSZ (12.83 GPa and 2.73 MPa√m), as shown in Table 2.[173–176] The mechanical strength can be improved without compromising the electrical conductivity by reduction-annealing the sample. In such a case, a compressed surface layer is formed by the chemical expansion that occurs during contact reduction of its surface.[177] Doping CeO_2 enhances the fracture toughness of the solid solution by promoting a greater extent of stress-induced tetragonal to monoclinic phase transformation.[178]

Table 2 A comparison of hardness and fracture toughness of some of the ceria-based electrolytes with those of 8-YSZ

Composition	Hardness (GPa)	Fracture toughness (MPa√m)
8-YSZ	12.83	2.73
GDC	5.46	1.16
$Ce_{0.8}Y_{0.2}O_2$	7.9	2.16
$Ce_{0.8}Sm_{0.2}O_2$	8.2	2.3
$Ce_{0.8}Sm_{0.1}Y_{0.1}O_2$	8.34	2.28
$Gd_{0.1}Ce_{0.89}Ge_{0.01}O_{0.01}$	10.85	3.18
$Ce_{0.9}Sm_{0.1}O_{1.95}$	5.37	2.95

4. Approaches to improve conductivity and cell parameters

The reduction of Ce^{4+} to Ce^{3+} under low oxygen partial pressures leads to high electronic conductivity; therefore, they show low OCV and low efficiency due to the leakage current. Thus, there are different ways through which these problems could be solved. Some of the suggestions to solve the above issues related to ceria-based electrolytes are given in the following points:

(1) Nanomaterials and thin films can effectively improve the properties of ceria-based electrolytes. It is generally observed that compared to conventional single crystalline and polycrystalline materials, the ionic conductivities of nanocrystalline materials such as cubic zirconia, ceria and titania are much higher. It is reported that CeO_2 nanoparticles under high pressure exhibit an ionic conductivity of 3×10^{-3} S cm^{-1} at 300 °C under 5 GPa for 6 mol% SDC nanoparticles.[179,180] Apart from nanoparticles, GDC thin film electrolytes have a higher power density than YSZ electrolytes. This is due to the higher conductivity of the GDC electrolyte against that of the YSZ electrolyte and the expansion of the electrochemical reaction zone. The improved ionic conductivity increases the oxygen transport rate at the electrolyte–electrode interface, which reduces the electrode overpotential. The surface area availability increases significantly in nanoparticles compared to bulk materials.[181–183]

(2) Nanocomposite electrolyte materials have the potential for use in LT-SOFCs due to their high ionic conductivity at low temperatures and low cost. Fundamentally, a typical nanocomposite ($CeO_{2-\delta}/CeO_2$, $GDC/CoFe_2O_4$, $YSZ/SrTiO_3$, *etc.*) consists of a core–shell type structure on a nano-scale. It has a core (ceria) and a salt (carbonate or another oxide) that develops a shell layer covering the core. The functionality of nanocomposites is determined by the interfaces between the constituent phases, which lead to fast ionic transport at the interfaces. Different ceria-based nanocomposites, such as ceria-carbonate, ceria-halide, ceria-sulphate, ceria-hydroxide, ceria-alumina and ceria-oxide, have been of significant interest for use as SOFC electrolyte materials.[116,184–186] Generally, ionic conductivity and power density of ceria-carbonate nanocomposites have been reported to be >0.1 S cm^{-1} at 300 °C and ~1000 mW cm^{-2} between 450 and 500 °C, respectively.[187] At slightly higher temperatures (600–650 °C), the protonic conductivity of $Sm_{0.2}Ce_{0.8}O_2–Na_2CO_3$ is reported to be ~0.044 S cm^{-1} with a power density of 281.5 mW cm^{-2}. These results are much higher than those of single-phase oxide proton-conducting electrolytes.[188] Shah *et al.* observed that a 10% coating of Na_2CO_3 on GDC generates appreciable O^{2-} vacancies compared to GDC.[180] This led to high power density (968 mW cm^{-2}) and high ionic conductivity (0.2 S cm^{-1} at 520 °C) with sufficient OCV (1.013 V). It was due to the formation of a composite core–shell heterostructure between GDC and amorphous Na_2CO_3. The formation of a junction suppressed the electronic conduction while enhancing the ionic transportation through the electrolyte membrane. A binary composite, $(Li/Na)_2CO_3$ – SDC, exhibited a high conductivity

and cell performance of 0.31 S cm^{-1} and 617 mW cm^{-2}, respectively, at 600 °C since the interface acted as a superionic highway, which enabled the transportation of ions.[189] Composites with SDC reach power densities as high as 640 and 760 mW cm^{-2} at low temperatures of 500 and 550 °C, respectively.[190] In another study, the addition of a $Ni_{0.8}Co_{0.15}Al_{0.05}Li$ membrane into $Ce_{0.8}Sm_{0.2}O_{2-\delta}$-$Na_2CO_3$ electrolyte eliminated the polarisation between different interfaces and resulted in a high-power density of 1072 mW cm^{-2} at 550 °C.[191] Compared to pure $NaFeO_2$, composites such as CeO_2-coated $NaFeO_2$ have a power output of 727 mW cm^{-2} and an OCV of 1.06 V at 550 °C. This is due to the hetero-interfaces between $NaFeO_2$ and CeO_2 that provide a fast oxide ion conducting path and to CeO_2 that creates more oxygen vacancies for protonic transportation. Ionic conduction through the interface is much easier than structural bulk conduction. Principally, point defects in ceria-based materials are responsible for originating ionic charge carriers. Therefore, in LT-SOFCs, interface conduction should be promoted as a new approach for ion-conducting electrolytes.[192,193]

(3) Another solution is to make use of electron-blocking layers. A $BaCeO_3$–Ni-based composite anode achieves higher OCV due to the reaction of diffused Ba ions with doped ceria electrolyte during the sintering process, forming an electron-blocking interlayer. This interlayer eliminates the problem of internal short-circuiting in doped ceria electrolytes. Apart from $BaCeO_3$, ZrO_2, Bi_2O_3, and $SrCeO_3$ are used as electron-blocking layers.[79,194] Another way to solve the short-circuiting problem is to use the bi- and tri-layer electrolyte strategy. The bi-layer electrolyte strategy uses a pure oxygen ion-conducting YSZ layer to block electron conduction. On the other hand, the tri-layer electrolyte system consists of a GDC layer on the anode side, a YSZ electron-blocking layer in the middle and a second GDC buffer layer on the cathode side.[195] In a tri-layer electrolyte system, the first dense GDC electrolyte is fabricated by co-sintering a thin, screen-printed GDC layer with an anode support (NiO-8YSZ substrate and a NiO-GDC anode). In contrast, the two electrolyte layers are deposited *via* physical vapour deposition. For a tri-doped electrolyte system, the electrolyte resistance is only 0.01 Ω cm^{-2} with a power density of 1.2 W cm^{-2} at 650 °C.[195] However, problems with low ionic conductivity, low chemical and mechanical stability, undesirable solid solutions, and thermal mismatch of the multilayer electrolytes pose issues in utilising the electron-blocking layer method.[194]

(4) A new approach was proposed wherein surface doping of Al^{3+} into Ce^{4+} created surface defects and surface O^{2-} vacancies at the interface of $CeAlO_2$. This approach enhanced the ionic conductivity (0.19 S cm^{-1}) and power density (1020 mW cm^{-2}) at 520 °C. It was observed that surface doping required band alignment between CeO_2 and $CeAlO_2$ due to the difference in the Fermi level. This established a space charge region constituting a built-in field, enhancing charge transportation and minimising e-conduction.[196] Co-doping and tri-doping have effectively been observed to reduce the sintering temperature and enhance the conductivity of ceria-based electrolytes, as observed from the data listed in Table 1. They generate higher oxygen vacancies than single-cation doping, resulting in higher diffusion due to minimum distortion. Also, ceria-based composites have high conductivities.

Based on the solutions mentioned above, it can be concluded that ceria-based materials show enhanced properties when used in doped, composites, bilayered and hetero-structured composite forms. Nanocomposites, electron-blocking layered structures and surface doping in CeO_2 resulted in very high power densities of >1000 mW cm^{-2}, thereby increasing the long-term stability of these oxides.

5. Conclusion and future direction for research

Solid oxide fuel/electrolyser cells (SOFCs/SOECs) are versatile and multipurpose devices that produce electricity, water, hydrogen and oxygen for different applications. The electrolyte is an essential and integral part of an SOFC. The present article discusses the different aspects that affect the ionic conductivity of ceria-based electrolytes for LT- and IT-SOFCs to make them cost-effective and increase their commercial viability. Gadolinium-doped ceria (GDC) and samarium-doped ceria (SDC) are very good and suitable ionic conducting electrolyte materials for LT- and IT-SOFCs due to the comparable ionic radii of Gd^{3+} ($r_{\text{ionic}} = 0.938$ Å) and Sm^{3+} ($r_{\text{ionic}} = 0.958$ Å) to Ce^{4+} ($r_{\text{ionic}} = 0.87$ Å). The solid solubility limit of both dopants is the highest compared to that of other dopants. However, a high concentration of dopants leads to secondary phase formations and clustering of oxygen vacancies, reducing ionic conductivity.

Different approaches can be used to increase the solid solubility of the dopants, optimise the microstructure and prevent the reduction of Ce^{4+} to Ce^{3+}. Surface engineering, chemical routes and thin film technology can be used to address these issues. Apart from the processing methods, different mechanisms such as utilising multi-dopants, nanocomposites, electron-blocking layers, and $CeO_{2-\delta}/CeO_2$ composites improve the conductivity of ceria-based electrolytes significantly. The densification of the electrolytes can be achieved by using sintering aids, particularly the addition of small amounts of alkali and alkaline earth metal oxides during processing. Alkali metal oxides increase the liquid phase sintering and wettability of CeO_2, while alkaline earth metal oxides avoid the reduction of cerium. As a future prospect, double dopants (alkali and alkaline earth oxides) could be beneficial to achieve high density with a reduced chance of cerium reduction in doped CeO_2 electrolyte. Additionally, studies on small quantities of nano-size sintering aids and sintering of composites, *i.e.* two suitable ionic conducting materials (doped CeO_2-bismuth vanadate, doped CeO_2–$LaAlO_3$, *etc.*) at appropriate temperatures and durations can be synthesised to obtain highly dense electrolytes for LT- and IT-SOFCs. Using double-layered electrolytes such as GDC-YSZ can also be a good approach to reduce interface-related issues with improved conductivity. Proton-conducting electrolytes could also be explored as electrolytes for intermediate temperature SOFCs/SOECs.

Data availability

The datasets used to support the findings of this study are available in the referenced publications.

Author contributions

Paramvir Kaur – conceptualization; data curation; formal analysis; visualization; writing-original draft. K. Singh – conceptualization; funding acquisition; supervision; validation; visualization; writing-review & editing.

Conflicts of interest

There are no conflicts of interest to declare.

Acknowledgements

The authors acknowledge the funding received from the Department of Science and Technology (DST), Government of India, through the Hydrogen and Fuel Cell (HFC)-2018 scheme [Project no. DST/TMD/HFC/2k18/123].

References

1 C. M. de Leon, P. Molina, C. Rios and J. J. Brey, Green hydrogen production's impact on sustainable development goals, *Int. J. Hydrogen Energy*, 2025, **142**, 642–653.

2 M. Bampaou and K. D. Panopoulos, An overview of hydrogen valleys: Current status, challenges and their role in increased renewable energy penetration, *Renewable Sustainable Energy Rev.*, 2025, **207**, 114923.

3 M. El-Adawy, I. B. Dalha, M. A. Ismael, Z. A. Al-Absi and M. A. Nemitallah, Review of Sustainable Hydrogen Energy Processes: Production, Storage, Transportation, and Color-Coded Classifications, *Energy Fuels*, 2024, **38**(23), 22686–22718.

4 B. S. Zainal, P. J. Ker, H. Mohamed, H. C. Ong, I. M. R. Fattah, S. M. A. Rahman, L. D. Nghiem and T. M. I. Mahlia, Recent advancement and assessment of green hydrogen production technologies, *Renewable Sustainable Energy Rev.*, 2024, **189**(A), 113941.

5 R. M. Ormerod, Solid oxide fuel cells, *Chem. Soc. Rev.*, 2003, **32**, 17–28.

6 A. J. Jacobson, Materials for Solid Oxide Fuel Cells, *Chem. Mater.*, 2010, **22**, 660–674.

7 P. Kaur and K. Singh, Review of perovskite-structure related cathode materials for solid oxide fuel cells, *Ceram. Int.*, 2020, **46**(5), 5521–5535.

8 Q. Xu, G. Zengjia, X. Lingchao, H. Qijiao, L. Zheng, B. T. Idris, Z. Keqing and N. Meng, A comprehensive review of solid oxide fuel cells operating on various promising alternative fuels, *Energy Convers. Manage.*, 2022, **253**, 115175.

9 A. B. Stambouli and E. Traversa, Solid oxide fuel cells (SOFCs): a review of an environmentally clean and efficient source of energy, *Renewable Sustainable Energy Rev.*, 2002, **6**(5), 433–455.

10 K. Singh and T. Walia, Review on silicate and borosilicate-based glass sealants and their interaction with components of solid oxide fuel cell, *Int. J. Energy Res.*, 2021, 1–24.

11 M. T. Mehran, M. Z. Khan, R. H. Song, T. H. Lim, M. Naqvi, R. Raza, B. Zhu and M. B. Hanif, A comprehensive review on durability improvement of solid oxide fuel cells for commercial stationary power generation systems, *Appl. Energy*, 2023, **352**, 121864.

12 X. Shao, R. A. Budiman, T. Sato, M. Yamaguchi, T. Kawada and K. Yashiro, Review of factors affecting the performance degradation of Ni-YSZ fuel electrodes in solid oxide electrolyzer cells, *J. Power Sources*, 2024, **609**, 234651.

13 N. Ai, Y. Zou, Z. Chen, K. Chen and S. P. Jiang, Progress on direct assembly approach for in situ fabrication of electrodes of reversible solid oxide cells, Mater. Rep, *Energy*, 2021, **1**, 100023.

14 M. Xu, R. Cao, H. Qin, N. Zhang, W. Yan, L. Liu, J. T. S. Irvine and D. Chen, Exsolved materials for CO_2 reduction in high-temperature electrolysis cells, Mater. Rep, *Energy*, 2023, **3**, 100198.

15 L. A. Omeiza, K. A. Kuterbekov, A. Kabyshev, K. Bekmyrza, M. Kubenova, S. Afroze, S. A. Bakar and A. K. Azad, Limitations and trends on cobalt-free cathode materials development for intermediate-temperature solid oxide fuel cell- an updated technical review, *Emergent Mater.*, 2024, **7**, 2189–2204.

16 L. A. Jolaoso, I. T. Bello, O. A. Ojelade, A. Yousuf, C. Duan and P. Kazempoor, Operational and scaling-up barriers of SOEC and mitigation strategies to boost H_2 production-a comprehensive review, *Int. J. Hydrogen Energy*, 2023, **48**, 33017–33041.

17 P. Iora and P. Chiesa, High efficiency process for the production of pure oxygen based on solid oxide fuel cell-solid oxide electrolyzer technology, *J. Power Sources*, 2009, **190**, 408–416.

18 M. Wang, K. M. Nowicki and J. T. S. Irvine, A Novel Solid Oxide Electrochemical Oxygen Pump for Oxygen Therapy, *J. Electrochem. Soc.*, 2022, **169**, 064509.

19 T. Raza, J. Yang, R. Wang, C. Xia, R. Raza, B. Zhu and S. Yun, Recent advance in physical description and material development for single component SOFC: A mini-review, *J. Chem. Eng.*, 2022, **444**, 136533.

20 N. Mahato, A. Banerjee, A. Gupta, S. Omar and K. Balani, Progress in Material Selection for Solid Oxide Fuel Cell Technology: A Review, *Prog. Mater. Sci.*, 2015, **72**, 141–337.

21 F. S. da Silva and T. M. de Souza, Novel materials for solid oxide fuel cell technologies: A literature review, *Int. J. Hydrogen Energy*, 2017, **42**(41), 26020–26036.

22 P. Vinchhi, M. Khandla, K. Chaudhary and R. Pati, Recent advances on electrolyte materials for SOFC: A review, *Inorg. Chem. Commun.*, 2023, **152**, 110724.

23 S. P. S. Shaikh, A. Muchtar and M. R. Somalu, A review on the selection of anode materials for solid-oxide fuel cells, *Renewable Sustainable Energy Rev.*, 2015, **51**, 1–8.

24 S. Dwivedi, Solid oxide fuel cell: Materials for anode, cathode and electrolyte, *Int. J. Hydrogen Energy*, 2020, **45**(44), 23988–24013.

25 A. Ndubuisi, S. Abouali, K. Singh and V. Thangadurai, Recent advances, practical challenges, and perspectives of intermediate temperature solid oxide fuel cell cathodes, *J. Mater. Chem. A*, 2022, **10**, 2196–2227.

26 L. Fan, W. Luo, Q. Fan, Q. Hu, Y. Jing, T. W. Chiu and P. D. Lund, Status and outlook of solid electrolyte membrane reactors for energy, chemical, and environmental applications, *Chem. Sci.*, 2025, **16**, 6620–6687.

27 Y. Gao, M. Zhang, M. Fu, W. Hu, H. Tong and Z. Tao, A comprehensive review of recent progresses in cathode materials for Proton-conducting SOFCs, *Energ. Rev.*, 2023, **2**, 100038.

28 H. Inaba and H. Tagawa, Ceria-based solid electrolytes, *Solid State Ionics*, 1996, **83**, 1–16.

29 R. N. Basu, Materials for Solid Oxide Fuel Cells, in *Recent Trends in Fuel Cell Science and Technology*, ed. S. Basu, Springer, New York, 2007.

30 Z. Zakaria, M. A. Zuraida, H. A. H. Saiful and K. B. Yap, A review of solid oxide fuel cell component fabrication methods toward lowering temperature, *Int. J. Energy Res.*, 2020, **44**(2), 594–611.

31 G. Kaur, SOFC Technology: Its Working and Components, in *Solid Oxide Fuel Cell Components*, Springer, Cham, 2016, pp. 79–122.

32 S. D. Priya, A. I. Selvakumar and A. S. Nesaraj, Overview on Ceramic and Nanostructured Materials for Solid Oxide Fuel Cells (SOFCs) Working at Different Temperatures, *J. Electrochem. Sci. Technol.*, 2020, **11**(2), 99–116.

33 Z. Yang, Recent advances in metallic interconnects for solid oxide fuel cells, *Int. Mater. Rev.*, 2008, **53**(1), 39–54.

34 F. Smeacetto, A. De Miranda, A. Chrysanthou, E. Bernardo, M. Secco, M. Bindi, M. Salvo, A. G. Sabato and M. Ferraris, Novel Glass-Ceramic Composition as Sealant for SOFCs, *J. Am. Ceram. Soc.*, 2014, **97**, 3835–3842.

35 N. Caron, L. Bianchi and S. Methout, Development of a Functional Sealing Layer for SOFC Applications, *J. Therm. Spray Technol.*, 2008, **17**(5–6), 598–602.

36 J. W. Fergus, Sealants for solid oxide fuel cells, *J. Power Sources*, 2005, **147**, 46–57.

37 K. Sood, K. Singh and O. P. Pandey, Co-existence of cubic and orthorhombic phases in Ba-doped $LaInO_3$ and their effect on conductivity, *Physica B*, 2015, **456**, 250–257.

38 K. Sood, K. Singh, S. Basu and O. P. Pandey, Optical, thermal, electrical and morphological study of $La_{1-x}Ca_xGaO_{3-\delta}$ (x=0, 0.05, 0.10, 0.15 and 0.20) electrolyte, *J. Eur. Ceram. Soc.*, 2016, **36**(13), 3165–3171.

39 J. K. Gill, O. P. Pandey and K. Singh, Ionic conductivity, structural and thermal properties of pure and Sr^{2+} doped $Y_2Ti_2O_7$ pyrochlores for SOFC, *Solid State Sci.*, 2011, **13**, 1960–1966.

40 J. K. Gill, O. P. Pandey and K. Singh, Role of sintering temperature on thermal, electrical and structural properties of $Y_2Ti_2O_7$ pyrochlores, *Int. J. Hydrogen Energy*, 2011, **36**, 14943–14947.

41 M. Singh, J. K. Gill, S. Kumar and K. Singh, Preparation of $Y_2Ti_2O_7$ pyrochlore using high-energy ball milling and their structural, thermal and conducting properties, *Ionics*, 2012, **18**, 479–486.

42 J. K. Gill, O. P. Pandey and K. Singh, Ionic conductivity, structural and thermal properties of Ca^{2+} doped $Y_2Ti_2O_7$ pyrochlores for SOFC, *Int. J. Hydrogen Energy*, 2012, **37**, 3857–3864.

43 R. Kant, K. Singh and O. P. Pandey, Microstructural and electrical behavior of $Bi_4V_{2-x}Cu_xO_{11-\delta}$ ($0 \leq x \leq 0.4$), *Ceram. Int.*, 2009, **35**, 221–227.

44 R. Kant, K. Singh and O. P. Pandey, Structural, thermal and transport properties of $Bi_4V_{2-x}Ga_xO_{11-\delta}$ ($0 \leq x \leq 0.4$), *Ionics*, 2010, **16**, 277–282.

45 S. Omar, E. D. Wachsman and J. C. Nino, A co-doping approach towards enhanced ionic conductivity in fluorite-based electrolytes, *Solid State Ionics*, 2006, **177**, 3199–3203.

46 K. Prabhakaran, M. O. Beigh, J. Lakra, N. M. Gokhale and S. C. Sharma, Characteristics of 8 mol% yttria-stabilised zirconia powder prepared by spray drying process, *J. Mater. Process. Technol.*, 2007, **189**, 178–181.

47 J. Zhang, C. Lenser, N. H. Menzler and O. Guillon, Comparison of solid oxide fuel cell (SOFC) electrolyte materials for operation at 500°C, *Solid State Ionics*, 2020, **344**, 115138.

48 M. F. Öksüzömer, G. Dönmez, V. Sariboğa and T. G. Altinçekiç, Microstructure and ionic conductivity properties of gadolinia doped ceria ($Gd_xCe_{1-x}O_{2-x/2}$) electrolytes for intermediate temperature SOFCs prepared by the polyol method, *Ceram. Int.*, 2013, **39**, 7305–7315.

49 B. S. Prakash, R. Pavitra, S. S. Kumar and S. Aruna, Electrolyte bi-layering strategy to improve the performance of an intermediate temperature solid oxide fuel cell: A review, *J. Power Sources*, 2018, **381**, 136–155.

50 S. He, Y. Zou, K. Chen and S. P. Jiang, A critical review of key materials and issues in solid oxide cells, *Interdiscip. Mater.*, 2023, **2**, 111–136.

51 M. Choolaei, M. F. Vostakola and B. A. Horri, Recent Advances and Challenges in Thin-Film Fabrication Techniques for Low-Temperature Solid Oxide Fuel Cells, *Crystals*, 2023, **13**, 1008.

52 M. F. Vostakola, H. Ozcan, R. S. El-Emam and B. A. Horri, Recent Advances in High-Temperature Steam Electrolysis with Solid Oxide Electrolysers for Green Hydrogen Production, *Energies*, 2023, **16**, 3327.

53 Y. Zhang, R. Knibbe, J. Sunarso, Y. Zhong, W. Zhou, Z. Shao and Z. Zhu, Recent Progress on Advanced Materials for Solid-Oxide Fuel Cells Operating Below 500 °C, *Adv. Mater.*, 2017, 1700132.

54 B. Singh, S. Ghosh, S. Aich and B. Roy, Low temperature solid oxide electrolytes (LT-SOE): A review, *J. Power Sources*, 2017, **339**, 103–135.

55 S. Thakur, M. Devi and K. Singh, Structural and optical properties of La and Gd substituted $Bi_{4-x}M_xV_2O_{11-\delta}$ ($0.1 \leq x \leq 0.3$), *Ionics*, 2014, **20**, 73–81.

56 E. D. Wachsman, G. R. Ball, N. Jiang and D. A. Stevenson, Structural and defect studies in solid oxide electrolytes, *Solid State Ionics*, 1992, **52**, 213–218.

57 H. Shi, C. Su, R. Ran, J. Cao and Z. Shao, Electrolyte materials for intermediate-temperature solid oxide fuel cells, *Prog. Nat. Sci.: Mater. Int.*, 2020, **30**, 764–774.

58 M. F. Vostakola and B. A. Horri, Progress in Material Development for Low-Temperature Solid Oxide Fuel Cells: A Review, *Energies*, 2021, **14**, 1280.

59 R. Kant, K. Singh and O. P. Pandey, Synthesis and characterization of bismuth vanadate electrolyte material with aluminium doping for SOFC application, *Int. J. Hydrogen Energy*, 2008, **33**, 455–462.

60 S. Gupta and K. Singh, γ-Phase stabilized $Bi_4Ba_xV_{2-x}O_{11-\delta}$ ($0.0 \leq x \leq 0.20$): Structural, thermal and conducting properties, *Solid State Ionics*, 2015, **278**, 233–238.

61 T. Wei, P. Singh, Y. Gong, J. B. Goodenough, Y. Huang and K. Huang, $Sr_{3-3x}Na_{3x}Si_3O_{9-1.5x}$ ($x = 0.45$) as a superior solid oxide-ion electrolyte for intermediate temperature-solid oxide fuel cells, *Energy Environ. Sci.*, 2014, **7**, 1680–1684.

62 Y. Li, N. Mushtaq, Y. Chen, W. Ye, Z. Zhuang, M. Singh, Y. Jing and L. Fan, Revisiting Mo-Doped $SrFeO_{3-\delta}$ Perovskite: The Origination of Cathodic Activity and Longevity for Intermediate-Temperature Solid Oxide Fuel Cells, *Adv. Funct. Mater.*, 2025, **35**(3), 2411025.

63 E. Filonova and D. Medvedev, Recent progress in the design, characterisation and application of $LaAlO_3$-and $LaGaO_3$-based solid oxide fuel cell electrolytes, *Nanomaterial*, 2022, **12**, 1991.

64 J. Yu, H. Liu, X. Chen, J. Xing, B. Yuan, M. Wang and W. Ma, Ionic conductivity and crystal structure of LSGM with different element mole ratios, *Fuel Cells*, 2021, **21**, 149–154.

65 G. M. Rupp, M. Glowacki and J. Fleig, Electronic and ionic conductivity of $La_{0.95}Sr_{0.05}Ga_{0.95}Mg_{0.05}O_{3-\delta}$ (LSGM) single crystals, *J. Electrochem. Soc.*, 2016, **163**, F1189.

66 K. T. Bae, I. Jeong, D. Kim, H. Yu, H. N. Im, A. Akromjon, C. W. Lee and K. T. Lee, Highly active cobalt-free perovskites with Bi doping as bifunctional oxygen electrodes for solid oxide cells, *J. Chem. Eng.*, 2023, **461**, 142051.

67 I. Stijepovic, A. J. Darbandi and V. V. Srdic, Conductivity of Co and Ni doped lanthanum-gallate synthesized by citrate sol-gel method, *Ceram. Int.*, 2013, **39**, 1495–1502.

68 V. Thangadurai and W. Weppner, Studies on electrical properties of $La_{0.8}Sr_{0.2}Ga_{0.8}Mg_{0.2}O_{2.80}$ (LSGM) and LSGM-$SrSn_{1-x}Fe_xO_3$ ($x = 0.8$; 0.9) composites and their chemical reactivity, *Electrochim. Acta*, 2005, **50**, 1871–1877.

69 C. Sun, H. Li and L. Chen, Nanostructured ceria-based materials: synthesis, properties, and applications, *Energy Environ. Sci.*, 2012, **5**, 8475–8505.

70 N. Izu, N. Murayama, W. Shin, I. Matsubara and S. Kanzaki, Resistive Oxygen Sensors Using Cerium Oxide Thin Films Prepared by Metal Organic Chemical Vapor Deposition and Sputtering, *Jpn. J. Appl. Phys.*, 2004, **43**(10), 6920–6924.

71 I. Shajahan, H. P. Dasari and M. B. Saidutta, Effect of sintering aids on sintering kinetic behaviour of praseodymium doped ceria based electrolyte material for solid oxide cells, *Int. J. Hydrogen Energy*, 2020, **45**, 25935–25944.

72 E. Aneggi, M. Boaro, S. Colussi, C. de Leitenburg and A. Trovarelli, Ceria-Based Materials in Catalysis: Historical Perspective and Future Trends, in *Handbook on the Physics and Chemistry of Rare Earths*, 2016, vol. 50, pp. 209–242.

73 H. Shi, T. Hussain, R. Ahuja, T. W. Kang and W. Luo, Role of vacancies, light elements and rare-earth metals doping in CeO_2, *Sci. Rep.*, 2016, **6**, 31345.

74 J. P. Y. Tan, H. R. Tan, C. Boothroyd, Y. L. Foo, C. B. He and M. Lin, Three-Dimensional Structure of CeO_2 Nanocrystals, *J. Phys. Chem. C*, 2011, **115**, 3544–3551.

75 M. K. Mahapatra and K. Lu, Seal glass for solid oxide fuel cells, *J. Power Sources*, 2010, **195**, 7129–7139.

76 Y. P. Fu, J. Ouyang, C. H. Li and S. H. Hu, Chemical bulk diffusion coefficient of $Sm_{0.5}Sr_{0.5}CoO_{3-\delta}$ cathode for solid oxide fuel cells, *J. Power Sources*, 2013, **240**, 168–177.

77 P. Arunkumar, M. Meena and K. S. Babu, A review on cerium oxide-based electrolytes for ITSOFC, Nano, *Energy*, 2012, **1**(5), 288–305.

78 K. J. Hwang, M. Jang and M. K. Kim, *et. al*, Effective buffer layer thickness of La-doped CeO_2 for high durability and performance on $La_{0.9}Sr_{0.1}Ga_{0.8}Mg_{0.2}O_{3-\delta}$ electrolyte supported type solid oxide fuel cells, *J. Eur. Ceram. Soc.*, 2021, **41**, 2674–2681.

79 T. K. Maiti, J. Majhi, S. K. Maiti, J. Singh, P. Dixit, T. Rohilla, S. Ghosh, S. Bhushan and S. Chattopadhyay, Zirconia- and ceria-based electrolytes for fuel cell applications: critical advancements toward sustainable and clean energy production, *Environ. Sci. Pollut. Res.*, 2022, **29**, 64489–64512.

80 D. Ding, X. Li, S. Y. Lai, K. Gerdes and M. Liu, Enhancing SOFC cathode performance by surface modification through infiltration, *Energy Environ. Sci.*, 2014, **7**, 552–575.

81 S. C. Shirbhate, K. Singh and S. A. Acharya, Review on local structural properties of ceria-based electrolytes for IT-SOFC, *Ionics*, 2017, **23**, 1049–1057.

82 Y. C. Wu and C. C. Lin, The microstructures and property analysis of aliovalent cations (Sm^{3+}, Mg^{2+}, Ca^{2+}, Sr^{2+}, Ba^{2+}) co-doped ceria-base electrolytes after an aging treatment, *Int. J. Hydrogen Energy*, 2014, **39**, 7988–8001.

83 G. Kim, N. Lee, K. B. Kim, B. K. Kim, H. Chang, S. J. Song and J. Y. Park, Various synthesis methods of aliovalent-doped ceria and their electrical properties for intermediate temperature solid oxide electrolytes, *Int. J. Hydrogen Energy*, 2013, **38**, 1571–1587.

84 T. Kaur, K. Singh and J. Kolte, Influence of Sr doping on structural and electrical properties of ceria and performance of a single solid oxide fuel cell, *Ionics*, 2024, 1–16.

85 M. S. Arshad, X. Y. Mbianda and C. Billing, Investigating the physico-chemical and electrochemical properties of various aliovalent cations doped ceria powders for electrolytic applications in solid oxide fuel cells, *Int. J. Hydrogen Energy*, 2024, **52**(D), 1172–1181.

86 K. Pathmanathan, P. Iyngaran, P. Abiman and N. Kuganathan, Defect Engineering and Dopant Properties of $MgSiO_3$, *Eng*, 2025, **6**, 51.

87 H. Yahiro, T. Ohuchi, K. Eguchi and H. Arai, Electrical properties and microstructure in the system ceria-alkaline earth oxide, *J. Mater. Sci.*, 1988, **23**, 1036–1041.

88 M. Kahlaoui, S. Chefi, A. Inoubli, A. Madani and C. Chefi, Synthesis and electrical properties of co-doping with La^{3+}, Nd^{3+}, Y^{3+}, and Eu^{3+} citric acid-nitrate prepared samarium-doped ceria ceramics, *Ceram. Int.*, 2013, **39**, 3873–3879.

89 N. Jaiswal, S. Upadhyay, D. Kumar and O. Parkash, Sm^{3+} and Sr^{2+} co-doped ceria prepared by citrate-nitrate auto-combustion method, *Int. J. Hydrogen Energy*, 2014, **39**, 543–551.

90 A. V. C. Aldridge and R. T. Baker, Ionic conductivity in multiply substituted ceria-based electrolytes, *Solid State Ionics*, 2018, **316**, 9–19.

91 T. Kaur, K. Singh and J. Kolte, Process parameters and their effect on the structure and morphology of gadolinium-doped ceria, *Mater. Today: Proc.*, 2023, **80**(2), 937–941.

92 T. Kaur, K. Singh and J. Kolte, Effect of Intrinsic and Extrinsic Oxygen Vacancies on the Conductivity of Gd-Doped CeO_2 Synthesized by a Sonochemical Route, *J. Phys. Chem. C*, 2022, **126**(42), 18018–18028.

93 N. Mahato, A. Gupta and K. Balani, Doped zirconia and ceria-based electrolytes for solid oxide fuel cells: a review, *Nanomater. Energy*, 2012, **1**(1), 27–45.

94 G. Accardo, L. Spiridigliozzi, R. Cioffi, C. Ferone, E. Di Bartolomeo, S. P. Yoon and G. Dell'Agli, Gadolinium-doped ceria nanopowders synthesized by urea-based homogeneous co-precipitation (UBHP), *Mater. Chem. Phys.*, 2017, **187**, 149–155.

95 P. R. Alvarez, M. V. Castrejón, G. González, M. Cassir, C. F. Morales and J. C. Carvayar, Ceria-based electrolytes with high surface area and improved conductivity for intermediate temperature solid oxide fuel cells, *J. Mater. Sci.*, 2017, **52**, 519–532.

96 S. Shirbhate, R. N. Nayyar, P. K. Ojha, A. K. Yadav and S. Acharya, Exploration of Atomic Scale Changes during Oxygen Vacancy Dissociation Mechanism in Nanostructure Co-Doped Ceria: As Electrolytes for IT-SOFC, *J. Electrochem. Soc.*, 2019, **166**(8), F544–F554.

97 S. K. Anirban and A. Dutta, Revisiting ionic conductivity of rare earth doped ceria: Dependency on different factors, *Int. J. Hydrogen Energy*, 2020, **45**(46), 25139–35166.

98 C. E. Milliken and S. Guruswamy, Electrochemical Stability of Strontium-Doped Ceria Electrolyte in Solid-Oxide Fuel Cell Applications, *J. Am. Ceram. Soc.*, 2001, **84**(7), 1533–1538.

99 J. E. Hong, S. Ida and T. Ishihara, Effects of transition metal addition on sintering and electrical conductivity of La-doped CeO_2 as buffer layer for doped $LaGaO_3$ electrolyte film, *Solid State Ionics*, 2014, **262**, 374–377.

100 J. Zhang, C. Ke, H. Wu, J. Yu, J. Wang and Y. Wang, Solubility limits, crystal structure and lattice thermal expansion of Ln_2O_3 (Ln=Sm, Eu, Gd) doped CeO_2, *J. Alloys Compd.*, 2017, **718**, 85–91.

101 V. Raghavan, *Materials Science and Engineering*, 6th edn, PHL Learning Private Limited, Delhi, 2015.

102 M. Takacs, J. R. Scheffe and A. Steinfeld, Oxygen nonstoichiometry and thermodynamic characterization of Zr doped ceria in the 1573-1773 K temperature range, *Phys. Chem. Chem. Phys.*, 2015, **17**, 7813–7822.

103 M. Coduri, S. Checchia, M. Longhi, D. Ceresoli and M. Scavini, Rare Earth Doped Ceria: The Complex Connection Between Structure and Properties, *Front. Chem.*, 2018, **6**, 526.

104 T. A. Ring, *Fundamentals of Ceramic Powder Processing and Synthesis*, Elsevier Science, 1996.

105 M. A. Khan, E. Haq, M. S. Javed, C. Xu, S. S. A. Shah, M. A. Nazir, M. Imran, M. A. Assiri, A. Ahmad and S. Hussain, Facile synthesis of ceria-based composite oxide materials by combustion for high-performance solid oxide fuel cells, *Ceram. Int.*, 2021, **47**, 22035–22041.

106 A. Paulus, S. Kammler, S. Heuer, M. C. Paulus, P. Jakes, J. Granwehr and R. A. Eichel, Sol Gel vs. Solid State Synthesis of the Fast Lithium-Ion Conducting Solid State Electrolyte $Li_7La_3Zr_2O_{12}$ Substituted with Iron, *J. Electrochem. Soc.*, 2019, **166**(3), A5403–A5409.

107 J. Kim, Q. Mistarihi and H. J. Ryu, Grain Size and Porosity Controlling of CeO_2 for Surrogate of UO_2 Fuel and Fracture Toughness Calculation, *Transactions of the Korean Nuclear Society Autumn Meeting*, 2019, pp. 1–5.

108 C. Zhao, C. Z. Zhao, M. Werner, S. Taylor, P. Chalker and P. King, Grain size dependence of dielectric relaxation in cerium oxide as high-k layer, *Nano. Res. Lett.*, 2013, **8**, 172.

109 I. Shajahan, J. Ahn, P. Nair, S. Medisetti, S. Patil, V. Niveditha, G. U. B. Babu, H. P. Dasari and J. H. Lee, Praseodymium doped ceria as electrolyte material for IT-SOFC applications, *Mater. Chem. Phys.*, 2018, **216**, 136–142.

110 P. L. Chen and I. W. Chen, Grain Growth in CeO_2: Dopant Effects, Defect Mechanism, and Solute Drag, *J. Am. Ceram. Soc.*, 1996, **79**(7), 1793–1800.

111 S. Y. Toor and E. Croiset, Reducing sintering temperature while maintaining high conductivity for SOFC electrolyte: Copper as sintering aid for Samarium Doped Ceria, *Ceram. Int.*, 2019, **46**(1), 1148–1157.

112 J. D. Nicholas and L. C. De Jonghe, Prediction and evaluation of sintering aids for Cerium Gadolinium Oxide, *Solid State Ionics*, 2007, **178**(19–20), 1187–1194.

113 P. Kaur and K. Singh, Perovskite-structured cobalt-free cathode materials for solid oxide fuel cells, in *Recent Advances in Renewable Energy Technologies*, ed. M. Jeguirim, Academic Press, Cambridge, 2022, vol. 2, pp. 357–373.

114 A. Tschope and R. Birringer, Grain Size Dependence of Electrical Conductivity in Polycrystalline Cerium Oxide, *J. Electroceram.*, 2001, **7**, 169–177.

115 D. E. P. Martinez, J. A. D. Guillen, S. M. Montemayor, J. C. DGuillen, O. B. Diaz, M. E. B. Medellin, M. R. D. Guillen and A. F. Fuentes, High ionic conductivity in CeO_2 SOFC solid electrolytes; effect of Dy doping on their electrical properties, *Int. J. Hydrogen Energy*, 2020, **45**, 14062–14070.

116 B. Wang, B. Zhu, S. Yun, W. Zhang, C. Xia, M. Afzal, Y. Cai, Y. Liu, Y. Wang and H. Wang, Fast ionic conduction in

semiconductor $CeO_{2-\delta}$ electrolyte fuel cells, *NPG Asia Mater.*, 2019, **11**(51), 1–12.

117 G. Accardo, C. Ferone, R. Cioffi, D. Frattini, L. Spiridigliozzi and G. Dell'Agli, Electrical and microstructural characterization of ceramic gadolinium-doped ceria electrolytes for ITSOFCs by sol-gel route, *J. Appl. Biomater. Funct. Mater.*, 2016, **14**(1), e35–e41.

118 G. Dell'Agli, G. Mascolo, M. C. Mascolo and C. Pagliuca, Drying effect on thermal behavior and structural modifications of hydrous zirconia gel, *J. Am. Ceram. Soc.*, 2008, **91**(10), 3375–3379.

119 A. Dupont, C. Parent, B. L. Garrec and J. M. Heintz, Size and morphology control of Y_2O_3 nanopowders via a sol-gel route, *J. Solid State Chem.*, 2003, **171**(1–2), 152–160.

120 A. Sutka and G. Mezinskis, Sol-gel auto-combustion synthesis of spinel-type ferrite nanomaterials, *Front. Mater. Sci.*, 2012, **6**(2), 128–141.

121 W. Chen, F. Li and J. Yu, Combustion synthesis and characterization of nanocrystalline CeO_2-based powders via ethylene glycol-nitrate process, *Mater. Lett.*, 2006, **60**(1), 57–62.

122 T. Mahata, G. Das, R. K. Mishra and B. P. Sharma, Combustion synthesis of gadolinia doped ceria powder, *J. Alloys Compd.*, 2005, **391**(1), 129–135.

123 S. Kulkarni, S. Duttagupta and G. Phatak, Study of glycine nitrate precursor method for the synthesis of gadolinium doped ceria ($Ce_{0.8}Gd_{0.2}O_{1.90}$) as an electrolyte for intermediate temperature solid oxide fuel cells, *RSC Adv.*, 2014, **4**(87), 46602–46612.

124 M. F. L. Garcia, A. J. M. Araujo, R. A. Raimundo, R. M. Nascimento, J. P. F. Grilo and D. A. Macedo, Electrical properties of Ca-doped ceria electrolytes prepared by proteic sol-gel route and by solid-state reaction using mollusk shells, *Int. J. Hydrogen Energy*, 2021, **46**, 17374–17387.

125 B. Dunn, G. C. Farrington and B. Katz, Sol-gel approaches for solid electrolytes and electrode materials, *Solid State Ionics*, 1994, **70/71**, 3–10.

126 A. E. Danks, S. R. Hall and Z. Schnepp, The evolution of 'sol-gel' chemistry as a technique for materials synthesis, *Mater. Horiz.*, 2016, **3**, 91–112.

127 K. A. Bhabu, J. Theerthagiri, J. Madhavan, T. Balu, G. Muralidharan and T. R. Rajasekaran, Cubic fluorite phase of samarium doped cerium oxide $(CeO_2)_{0.96}Sm_{0.04}$ for solid oxide fuel cell electrolyte, *J. Mater. Sci.: Mater. Electron.*, 2016, **27**, 1566–1573.

128 M. Stojmenovic, N. Nisic, M. Kragovic, J. Gulicovski, F. Basoli, D. Bajuk-Bogdanovic and M. Zunic, Multidoped CeO_2 single-phase as electrolyte for IT-SOFC, *Solid State Ionics*, 2024, **414**, 116645.

129 G. Accardo, D. Frattini, H. C. Ham, J. H. Han and S. P. Yoon, Improved microstructure and sintering temperature of bismuth nano-doped GDC powders synthesized by direct sol-gel combustion, *Ceram. Int.*, 2018, **44**(4), 3800–3809.

130 A. Zarkov, A. Stanulis, T. Salkus, A. Kezionis, V. Jasulaitiene, R. Ramanauskas, S. Tautkus and A. Kareiva, Synthesis of nanocrystalline gadolinium doped ceria via sol-gel combustion and sol-gel synthesis routes, *Ceram. Int.*, 2016, **42**(3), 3972–3988.

131 D. A. Macedo, R. P. S. Dutra, R. M. Nascimento, J. M. Sasaki, M. R. Cesario, S. Rajesh, F. L. Figueiredo and F. M. B. Marques, Synthesis of $Ce_{0.8}Sm_{0.2}O_{1.9}$ solid electrolyte by a proteic sol-gel green method, *Cryst. Res. Technol.*, 2016, **51**(6), 400–404.

132 B. C. Steele, Appraisal of $Ce_{1-y}Gd_yO_{2-y/2}$ electrolytes for IT-SOFC operation at 500 °C, *Solid State Ionics*, 2000, **129**, 95–110.

133 S. Sulekar, M. Mehr, J. H. Kim and J. C. Nino, Effect of Reduced Atmosphere Sintering on Blocking Grain Boundaries in Rare-Earth Doped Ceria, *Inorganics*, 2021, **9**, 1–12.

134 S. Ramesh and G. Rajitha, Structural characterization and electrical properties of $Ce_{1-x}Sm_xO_{2-\delta}$ by sucrose-pectin-assisted auto combustion process, *Ionics*, 2020, **26**, 5089–5098.

135 A. Arabaci, Synthesis and characterization of Pr/Gd co-doped ceria by using the citric acid-nitrate combustion method, *Solid State Ionics*, 2018, **326**, 69–76.

136 H. P. Dasari, K. Ahn, S. Y. Park, J. Hong, H. Kim, K. J. Yoon, J. W. Son, B. K. Kim, H. W. Lee and J. H. Lee, Record-low sintering-temperature (600 °C) of solid-oxide fuel cell electrolyte, *J. Alloys Compd.*, 2016, **672**, 397–402.

137 R. O. Calderon, C. G. Mayer and H. Danninger, Fundamentals of Sintering: Liquid Phase Sintering, in *Encyclopedia of Materials: Metals and Alloys*, ed. F. G. Caballero, Elsevier, 2022, pp. 481–492.

138 C. G. M. Lima, T. H. Santos, J. P. F. Grilo, R. P. S. Dutra, R. M. Nascimento, S. Rajesh, F. C. Fonseca and D. A. Macedo, Synthesis and properties of CuO-doped $Ce_{0.9}Gd_{0.1}O_{2-\delta}$ electrolytes for SOFCs, *Ceram. Int.*, 2015, **41**(3), 4161–4168.

139 P. Kaur and K. Singh, Structural, thermal and electrical study of copper doped strontium zirconate, *Ionics*, 2020, **26**, 6233–6244.

140 J. Zolhafizi, M. A. Azmi, H. A. Rahman, H. Zakaria, S. Hassan, S. Mahzan, A. Ismail, A. M. T. Ariffin, M. F. Tukimon, U. A. Yusof and N. A. Baharuddin, Samarium Doped Ceria (SDC) Electrolyte Modification by Sintering Aids Addition to Reducing Sintering Temperature: A Review, *J. Kejuruter.*, 2023, **35**(1), 65–76.

141 J. Cheng, R. Xu and Y. Shi, A strategy for improving sinterability and electrical properties of gadolinium-doped ceria electrolyte using calcium oxide additive, *J. Rare Earths*, 2021, **39**, 728–733.

142 F. Meng, N. Lin, T. Xia, J. Wang, Z. Shi, J. Lian, Q. Li, H. Zhao and F. Ma, Neodymium-doped ceria nanomaterials: facile low-temperature synthesis and excellent electrical properties for IT-SOFCs, *RSC Adv.*, 2013, **3**, 6290–6294.

143 H. O. Torun and S. Cakar, Thermal characterization of Er-doped and Er-Gd co-doped ceria-based electrolyte materials for SOFC, *J. Therm. Anal.*, 2018, **133**, 1233–1239.

144 M. R. Cesário, E. Savary, S. Marinel, B. Raveau and V. Caignaert, Synthesis and electrochemical performance

of $Ce_{1-x}Yb_xO_{2-x/2}$ solid electrolytes: The potential of microwave sintering, *Solid State Ionics*, 2016, **294**, 67–72.

145 N. Momin, J. Manjanna, S. Senthilkumar and S. T. Aruna, La-and Gd-Doped CeO_2 Nanoparticles as Electrolyte Materials for Intermediate Temperature Solid Oxide Fuel Cells, in *Recent Trends in Electrochemical Science and Technology*, ed. Mudali, U. K., Aruna, S. T., Nagaswarupa, H. P. and Rangappa, D., Springer, Singapore, 2022, vol. 15, pp. 127–137.

146 Z. Khakpour, A. A. Yuzbashi, A. Maghsodipour and K. Ahmadi, Electrical conductivity of Sm-doped CeO_2 electrolyte produced by two-step sintering, *Solid State Ionics*, 2012, **227**, 80–85.

147 Y. Shilong, L. Mengnan, Z. Yanwei, L. Chuanming, C. Xiaowei and Y. E. Zhupeng, Study of $Sm_{0.2}Ce_{0.8}O_{1.9}$ (SDC) electrolyte prepared by a simple modified solid-state method, *J. Rare Earths*, 2014, **32**(8), 767.

148 N. Jaiswal, N. K. Singh, D. Kumar and O. Parkash, Effect of strontium (Sr) doping on the conductivity of ceria, *J. Power Sources*, 2012, **202**, 78–84.

149 Q. Lu, X. Dong, Z. Zhu and Y. Dong, Effect of CuO doping on sinterability, mechanical and electrical properties of Sm-doped CeO_2 ceramic thick membrane solid electrolytes, *Ceram. Int.*, 2014, **40**(10A), 15545–15550.

150 J. Yang, B. Ji, J. Si, Q. Zhang, Q. Yin, J. Xie and C. Tian, Synthesis and properties of ceria based electrolyte for IT-SOFCs, *Int. J. Hydrogen Energy*, 2016, **41**, 15979–15984.

151 C. Madhuri, K. Venkataramana, J. Shanker and C. V. Reddy, Effect of La^{3+}, Pr^{3+}, and Sm^{3+} triple-doping on structural, electrical, and thermal properties of ceria solid electrolytes for intermediate temperature solid oxide fuel cells, *J. Alloys Compd.*, 2020, **849**, 156636.

152 S. Xie, Y. Liu, W. Xi, D. Zhou and J. Meng, Effect of Nd/Mg co-doping on the electrical properties of ceria-based electrolyte materials, *Mater. Res. Innovations*, 2017, **21**(2), 69–73.

153 Y. Zheng, H. Gu, H. Chen, L. Gao, X. Zhu and L. Guo, Effect of Sm and Mg co-doping on the properties of ceria-based electrolyte materials for IT-SOFCs, *Mater. Res. Bull.*, 2009, **44**, 775–779.

154 T. Kaur, J. Kolte and K. Singh, Defect-induced improved electrical performance of doped ceria for solid oxide fuel cell applications, *Ceram. Int.*, 2024, **50**(10), 17054–17062.

155 T. Li and Q. Shi, Structure, morphology and electrical conductivity of Sm and Bi codoped CeO_2 electrolytes synthesized by co-precipitation method, *J. Mater. Sci.: Mater. Electron.*, 2018, **29**, 13925–13930.

156 F. Altaf, R. Batool, R. Gill, G. Abbas, R. Raza, M. A. Khan, Z. Rehman and M. A. Ahmad, Synthesis and characterisation of Co-doped ceria-based electrolyte material for low temperature solid oxide fuel cell, *Ceram. Int.*, 2019, **45**(8), 10330–10333.

157 S. A. M. Ali, M. Anwar, A. M. Abdalla, M. R. Somalu and A. Muchtar, $Ce_{0.80}Sm_{0.10}Ba_{0.05}Er_{0.05}O_{2-\delta}$ multi-doped ceria electrolyte for intermediate temperature solid oxide fuel cells, *Ceram. Int.*, 2017, **43**(1), 1265–1271.

158 K. Venkataramana, C. Madhuri, Y. S. Reddy, G. Bhikshamaiah and C. V. Reddy, Structural, electrical and thermal expansion studies of tri-doped ceria electrolyte materials for IT-SOFCs, *J. Alloys Compd.*, 2017, **719**, 97–107.

159 K. Venkataramana, C. Madhuri, J. S. C. Madhusudan and C. V. Reddy, Microwave-sintered Pr^{3+}, Sm^{3+}, Gd^{3+} triple-doped ceria electrolyte material for IT-SOFC applications, *Ionics*, 2018, **24**, 3075–3084.

160 K. Venkataramana, C. Madhuri and C. V. Reddy, Triple-doped Ceria-Carbonate ($Ce_{0.82}La_{0.06}Sm_{0.06}Gd_{0.06}O_{2-\delta}$-(Li-Na)$_2CO_3$) nanocomposite solid electrolyte materials for LT-SOFC applications, *Ceram. Int.*, 2020, **46**(17), 27584–27594.

161 *Proc. 2nd Eur. SOFC Forum*, ed. H. P. Buchkremer, U. Diekmann, D. Stover and B. Thorstensen, Oberrohrdorf, Switzerland, 1996, p. 221.

162 F. Meschke and R. W. Steinbrech, *Proc. 6th Int. Symp. Solid Oxide Fuel Cells, PV 99-19*, ed. M. Dokiya and S. C. Singhal, The Electrochem. Soc., Pennington, NJ, 1999, p. 1047.

163 *Proc. 3rd Eur. SOFC Forum*, ed. R. Vassen, R. W. Steinbrech, F. Tietz, D. Stover and P. Stevens, Oberrohrdorf, Switzerland, 1998, p. 557.

164 A. Rafique, R. Raza, N. A. Arifin, M. K. Ullah, A. Ali and R. S. Wilckens, Electrochemical and Thermal Characterization of Doped Ceria Electrolyte with Lanthanum and Zirconium, *Ceram. Int.*, 2018, **44**(6), 6493–6499.

165 R. Kriyama and H. Kiriyama, Kouzoumukikagaku I (Structural inorganic chemistry I), *Kyoritu*, 1964, 127.

166 P. De, V. Du, S. J. Van Plessis and L. A. Tonder, Elastic constants of a NiO single crystal: I, *J. Phys. C:Solid State Phys.*, 1971, **4**, 1983–1987.

167 M. Mori, T. Yamamoto, H. Itoh, H. Inaba and H. Tagawa, Thermal expansion of nickel-zirconia anodes in solid oxide fuel cells during fabrication and operation, *J. Electrochem. Soc.*, 1998, **145**(4), 1374–1381.

168 S. Watanabe, S. Sukino, T. Miyasaka, K. Sato, K. Yashiro, T. Kawada and T. Hashida, Influences of Ni content and porosity on mechanical properties of Ni-YSZ composites under solid oxide fuel cell operating conditions, *J. Mater. Sci.*, 2020, **55**, 8679–8693.

169 C. Madhuri, K. Venkataramana, S. Ramesh, J. Shanker and C. V. Reddy, Investigation of Triple-doped Ceria-Based Composite Materials for LT-SOFC Applications, *J. Electron. Mater.*, 2022, **51**, 5908–5918.

170 M. Morales, J. J. Roa, J. M. Perez-Falcón, A. Moure, J. Tartaj, F. Espiell and M. Segarra, Correlation between electrical and mechanical properties in $La_{1-x}Sr_xGa_{1-y}Mg_yO_{3-\delta}$ ceramics used as electrolytes for solid oxide fuel cells, *J. Power Sources*, 2014, **246**, 918–925.

171 C. K. Ng, S. Ramesh, C. Y. Tan, A. Muchtar and M. R. Somalu, Microwave sintering of ceria-doped scandia stabilized zirconia as electrolyte for solid oxide fuel cell, *Int. J. Hydrogen Energy*, 2016, **41**, 14184–14190.

172 A. Kishimoto, T. Umemura, S. Kondo and T. Teranishi, Ceria-based solid electrolyte exhibits superior mechanical

and electric properties compared to zirconia-based solid electrolyte, *Ceram. Int.*, 2022, **48**(15), 21824–21831.

173 S. Sameshima, T. Ichikawa, M. Kawaminami and Y. Hirata, Thermal and mechanical properties of rare earth-doped ceria ceramics, *Mater. Chem. Phys.*, 1999, **61**, 31–35.

174 M. Dudek, Ceramic oxide electrolytes based on CeO_2-Preparation, properties and possibility of application to electrochemical devices, *J. Eur. Ceram. Soc.*, 2008, **28**, 965–971.

175 R. V. Mangalaraja, S. Ananthakumar, A. Schachtsiek, M. Lopez, C. P. Camurri and R. E. Avila, Synthesis and mechanical properties of low temperature sintered, Sm^{3+} doped nanoceria electrolyte membranes for IT-SOFC applications, *Mater. Sci. Eng. A*, 2010, **527**, 3645–3650.

176 J. Cao, W. Liu and Y. Chen, Mechanical properties of plasma sprayed boron nitride nanoplatelet reinforced gadolinium-doped ceria (GDC) coating for intermediate temperature solid electrolyte, IOP Conf. Series, *Mater. Sci. Eng.*, 2019, **631**, 022020.

177 A. Kishimoto, N. Ohmoto and T. Teranishi, Temporary reinforcement of ceria-based ceramics using chemical expansion and concomitant change in electrical properties, *Mater. Lett.*, 2020, **270**, 127712.

178 M. Borik, A. Chislov, A. Kulebyakin, E. Lomonova and F. Milovich, Effect of Ceria Doping on the Mechanical Properties and Phase Stability of Partially Samaria-Stabilized Zirconia Crystals, *Crystals*, 2024, **14**, 736.

179 H. Takamura, J. Kobayashi, N. Takahashi and M. Okada, Electrical conductivity of ceria nanoparticles under high pressure, *J. Electroceram.*, 2009, **22**, 24–32.

180 M. A. K. Y. Shah, Y. Lu, N. Mushtaq, M. Yousaf and B. Zhu, Doped ceria electrolyte rich in oxygen vacancies for boosting the fuel cell performance of LT-CFCs, *Int. J. Hydrogen Energy*, 2023, **4**(8), 12474–12484.

181 D. Pérez-Coll, J. C. Ruiz-Morales, D. Marrero-López, P. Núñez and J. R. Frade, Effect of sintering additive and low temperature on the electrode polarization of CGO, *J. Alloys Compd.*, 2009, **467**, 533–538.

182 V. V. Kharton, A. P. Viskup, F. M. Figueiredo, E. N. Naumovich, A. L. Shaula and F. M. B. Marques, Electrochemical properties of Pr-doped $Ce(Gd)O^{2-}$, *Mater. Lett.*, 2002, **53**, 160–164.

183 A. Solovyev, A. Shipilova, E. Smolyanskiy, S. Rabotkin and V. Semenov, The Properties of Intermediate-Temperature Solid Oxide Fuel Cells with Thin Film Gadolinium-Doped Ceria Electrolyte, *Membranes*, 2022, **12**, 896.

184 L. Fan, C. Wang, M. Chen and B. Zhu, Recent development of ceria-based (nano)composite materials for low temperature ceramic fuel cells and electrolyte-free fuel cells, *J. Power Sources*, 2013, **234**, 154–174.

185 Y. Zhang, D. Zhu, X. Jia, J. Liu, X. Li, Y. Z. Ouyang, Z. Li, X. Gao and C. Zhu, Novel n-i CeO_2/a-Al_2O_3 Heterostructure Electrolyte Derived from the Insulator a-Al_2O_3 for Fuel Cells, *ACS Appl. Mater. Interfaces*, 2023, **15**(1), 2419–2428.

186 Y. Zhang, D. Zhu, Z. Zhao, J. Liu, Y. Ouyang, J. Yu, Z. Liu, X. Bai, N. Wang, L. Zhuang, W. Liu and C. Zhu, Observation of Fast Low-Temperature Oxygen Ion Conduction in CeO_2/β''-Al_2O_3 Heterostructure, *Adv. Sci.*, 2024, **11**, 2401130.

187 R. Raza, B. Zhu, A. Rafique, M. R. Naqvi and P. Lund, Functional ceria-based nanocomposites for advanced low-temperature (300-600 °C) solid oxide fuel cell: A comprehensive Review, Mater, *Today Energy*, 2020, **15**, 100373.

188 G. Zhang, W. Li, W. Huang, Z. Cao, K. Shao, F. Li, C. Tang, C. Li, C. He, Q. Zhang and L. Fan, Strongly coupled $Sm_{0.2}Ce_{0.8}O_2$-Na_2CO_3 nanocomposite for low temperature solid oxide fuel cells: One-step synthesis and super interfacial proton conduction, *J. Power Sources*, 2018, **386**, 56–65.

189 A. Ali, A. Rafique, M. Kaleemullah, G. Abbas, M. A. Khan, M. A. Ahmad and R. Raza, The effect of alkali-carbonates (single, binary, and ternary) on doped ceria, a composite electrolyte for low temperature solid oxide fuel cells, *ACS Appl. Mater. Interfaces*, 2018, **10**(1), 806–818.

190 M. S. Sharif, S. Rauf, Z. Tayyab, M. A. Masood, Y. Tian, M. A. K. Y. Shah, A. N. Alodhayb, R. Raza and B. Zhu, High Proton Conductivity in $xCuO/(1\text{-}x)CeO_2$ Electrolytes Induced by CuO Self-Nucleation and Electron-Ion Coupling, *Adv. Sci.*, 2025, 2417421.

191 X. Zhou, J. Yang, R. Wang, W. Zhang, S. Yun and B. Wang, Advances in lithium-ion battery materials for ceramic fuel cells, *Energy Mater.*, 2022, **2**, 200041.

192 S. Dwivedi, Solid oxide fuel cell: Materials for anode, cathode and electrolyte, *Int. J. Hydrogen Energy*, 2020, **45**(44), 23988–24013.

193 Y. Xing, M. Akbar, M. Yousaf, M. A. K. Y. Shah, C. Xia, J. Gao and X. Wang, CeO_2 coated $NaFeO_2$ proton-conducting electrolyte for solid oxide fuel cell, *Int. J. Hydrogen Energy*, 2021, **46**(15), 9855–9860.

194 Y. Ling, X. Wang, Z. Ma, K. Wei, Y. Wu, M. Khan, K. Zheng, S. Shen and S. Wang, Review of experimental and modelling developments for ceria-based solid oxide fuel cells free from internal short circuits, *J. Mater. Sci.*, 2020, **55**, 1–23.

195 J. Zhang, C. Lenser, N. Russner, A. Weber, N. H. Menzler and O. Guillon, Boosting intermediate temperature performance of solid oxide fuel cells via a tri-layer ceria-zirconia-ceria electrolyte, *J. Am. Ceram. Soc.*, 2023, **106**, 93–99.

196 M. A. K. Y. Shah, Y. Lu, N. Mushtaq, M. Yousaf and B. Zhu, Doped ceria electrolyte rich in oxygen vacancies for boosting the fuel cell performance of LT-CFCs, *Int. J. Hydrogen Energy*, 2023, **48**, 12474–12484.